 doi:10.20944/preprints202007.0416.v1

Analytical solution of the SIR-model for the temporal evolution of epidemics. Part A: Time-independent reproduction factor

M. Kröger[1,*], R. Schlickeiser[2,3,**]
[1] *Polymer Physics, Department of Materials, ETH Zurich, Zurich CH-8093, Switzerland, ORCID 0000-0003-1402-6714*
[2] *Institut für Theoretische Physik, Lehrstuhl IV: Weltraum- und Astrophysik, Ruhr-Universität Bochum, D-44780 Bochum, Germany, ORCID 0000-0003-3171-5079*
[3] *Institut für Theoretische Physik und Astrophysik, Christian-Albrechts-Universität zu Kiel, Leibnizstr. 15, D-24118 Kiel, Germany*
(Dated: July 9, 2020)

We revisit the Susceptible-Infectious-Recovered/Removed (SIR) model which is one of the simplest compartmental models. Many epidemological models are derivatives of this basic form. While an analytic solution to the SIR model is known in parametric form for the case of a time-independent infection rate, we derive an analytic solution for the more general case of a time-dependent infection rate, that is not limited to a certain range of parameter values. Our approach allows us to derive several exact analytic results characterizing all quantities, and moreover explicit, non-parametric, and accurate analytic approximants for the solution of the SIR model for time-independent infection rates. We relate all parameters of the SIR model to a measurable, usually reported quantity, namely the cumulated number of infected population and its first and second derivatives at an initial time $t = 0$, where data is assumed to be available. We address the question on how well the differential rate of infections is captured by the Gauss model (GM). To this end we calculate the peak height, width, and position of the bell-shaped rate analytically. We find that the SIR is captured by the GM within a range of times, which we discuss in detail. We prove that the SIR model exhibits an asymptotic behavior at large times that is different from the logistic model, while the difference between the two models still decreases with increasing reproduction factor. This part A of our work treats the original SIR model to hold at all times, while this assumption will be released in part B. Releasing this assumption allows to formulate initial conditions incompatible with the original SIR model.

Keywords: coronavirus; statistical analysis; extrapolation; parameter estimation; epidemic spreading

I. INTRODUCTION

Several recent studies[1–4] have demonstrated that the normal or Gaussian distribution function for the temporal evolution of the daily number of new cases (deaths, or alternatively infections) at time t due to the COVID-19 pandemic disease provides quantitatively correct descriptions for the monitored rates in many different countries. If applied early enough at the beginning of the pandemic wave the Gauss model (GM) makes realistic and reliable predictions for the future evolution of the first wave. It has been argued that the assumption of a Gaussian time evolution is well justified by the central limit theorem of statistics,[3] an agent-based model,[4] a Taylor expansion,[4] or as a special case of the SIR model.[2] A motivation of the present manuscript was to provide more rigorous arguments in favor of using the GM to estimate the characteristics (peak time, height, and width) of a first epidemic wave well ahead of its climax.

On our way we discovered a new analytical solution of the standard SIR-model[5–10] without vital dynamics describing the temporal evolution of the COVID-19 pandemic disease that applies to the whole range of parameters. This solution allows for an arbitrary time dependence of the infection and recovery rates but assumes that the ratio of the two rates is independent of time. This case generalizes earlier treatments where time-independent infection and recovery rates were adopted. Moreover, in contrast to earlier work we will also calculate analytically the daily differential rate of newly infected persons resulting from the SIR-model which is the key quantity to compare with the monitored data in different countries, as the size of the currently infected, and not yet recovered, compartment is usually not known. Its asymptotic behavior, peak time and peak amplitudes will all be obtained analytically and exactly.

Besides providing analytic expressions for the quantities characterizing the solution of the SIR model, we derive a simple, accurate approximant that can be used in practise, and shares all relevant features with the exact solution, as we will show. This is a stark improvement compared with approaches, where the solution of the SIR model was for example expanded into a divergent but asymptotic series,[11,12] or where it had been obtained assuming inequalities that do hold only within a very limited range of SIR parameters, as we will show.

As a side-observation we find that the SIR model exhibits an asymptotic behavior at large times that is qualitatively different from the logistic model, while the difference between the two models still decreases with increasing reproduction factor. Because the SIR model is sometimes used with arbitrary initial conditions, we recall here that initial conditions must be interrelated if the SIR model is assumed to hold at all times. This is the scenario to be investigated here, for reasons to be discussed in detail. The present investigation can be extended to the many variants of the SIR model.[13–21]

* mk@mat.etz.ch (M.K.), rsch@tp4.rub.de (R.S.)

Preprints (www.preprints.org) | NOT PEER-REVIEWED | Posted: 19 July 2020 doi:10.20944/preprints202007.0416.v1

II. SIR-MODEL

As the dynamics of the COVID-19 pandemic is much faster than the dynamics of births and deaths, the neglect of these demographic factors is well justified. The SIR system is the simplest of the compartmental models used for the mathematical modelling of infectious diseases. The considered population of $N \gg 1$ persons is assigned to the three compartments S (susceptible), I (infectious), or R (recovered/removed). Persons from the population may progress between these compartments.

A. Basic equations

In a fixed population of individuals let $I(t)$, $S(t)$ and $R(t)$ denote the infected, susceptible and recovered/removed fractions of persons involved in the infection at time t, so that

$$S(t) + I(t) + R(t) = 1 \tag{1}$$

and because S, I, R are fractions, they must all reside within the interval [0,1]. If $a(t)$ and $\mu(t)$ denote the semipositive time-dependent infection and recovery rates, respectively, the SIR-model is defined with the two dynamical equations[5,6,22]

$$\dot{I}(t) = a(t)S(t)I(t) - \mu(t)I(t) \tag{2}$$

$$\dot{S}(t) = -a(t)S(t)I(t). \tag{3}$$

where the dot here and in the following denotes a derivative with respect to t. The equation for the dynamics of $R(t)$ follows from the sum constraint (1), i.e.

$$\dot{R} = -\frac{d}{dt}[S(t) + I(t) - 1] = \mu(t)I(t), \tag{4}$$

where we inserted Eqs. (2) and (3). Eq. (3) can be written as

$$\frac{\dot{S}(t)}{S(t)} = \frac{d\ln S(t)}{dt} = -a(t)I(t), \tag{5}$$

so that

$$I(t) = -\frac{1}{a(t)}\frac{d\ln S(t)}{dt}, \tag{6}$$

implying that Eq. (4) becomes

$$\dot{R}(t) = -k(t)\frac{d\ln S(t)}{dt} \tag{7}$$

with the potentially time-dependent inverse reproduction factor

$$k(t) = \frac{\mu(t)}{a(t)} \tag{8}$$

The solution and its analytic approximant to be derived in this work holds for arbitrary $a(t)$, as long as $\mu(t)$ and $a(t)$ remain proportional to each other. In that case k is a constant, usually denoted as inverse basic reproduction number, $k = 1/R_0$.

B. Initial conditions: All-time versus semi-time SIR

There are two qualitative very different cases to be considered that can be regarded as equally valid approaches. We refer to these cases as the all-time case (I) and the semi-time case (II).

For the all-time case (A), treated by Kendall[6] and part A of this work, the ratio $k = \mu(t)/a(t)$ is regarded as identically constant at all times, from $t = -\infty$ to $t = \infty$. This implies, that one has to use boundary conditions $S(-\infty) = 1$, $I(-\infty) = 0$, $R(-\infty) = 0$ as the epidemy must not have existed at $t = -\infty$. For the special case of $k = 0$, $\mu(t) = 0$ and $R(t) = 0$ at all times according to Eq. (7), while Eqs. (1)–(3) reduce to $I(t) = 1 - S(t)$ and the simple logistic differential equation $\dot{S}(t) = -a(t)S(t)[1 - S(t)]$ determining all fractions analytically in terms of $a(t)$ (Appendix F).

For constant $k > 0$, Eq. (7) implies the important relation[6]

$$S(t) = S(t')e^{[R(t')-R(t)]/k} \tag{9}$$

valid for any choice of t and t'. Upon inserting the stated boundary conditions at $t' = -\infty$ into Eq (9), $S(t)$ and $R(t)$ are simply related via $S(t) = e^{-R(t)/k}$ or $R(t) = -k\ln S(t)$. A special case of this relationship is

$$S(0) = e^{-R(0)/k} \tag{10}$$

In view of Eq. (1), there remains the freedom to just specify one single initial condition at a certain $t = 0$, where data may have become available. One may regard the time $t = 0$ when the existence of the pandemic wave in the society is realized and monitoring of newly infected persons starts. Besides k there is thus a second parameter of the SIR model, which we denote by the positive ε as it usually represents a small number, but our results are valid for any ε. We define ε via the susceptible fraction of the population at time $t = 0$,

$$S(0) = e^{-\varepsilon} \tag{11}$$

There is no freedom for the remaining $R(0)$ and $I(0)$ if k is known. Inserting the above boundary conditions into Eq. (10), and making use of Eq. (1) one has

$$R(0) = k\varepsilon, \qquad I(0) = f_k(\varepsilon) \tag{12}$$

involving a function in $f_k(\varepsilon)$ that is going to frequently occur in this work

$$f_k(x) = 1 - kx - e^{-x} \tag{13}$$

Here $R(0)$ and $I(0)$ represent the recovered/removed and infected fractions of the population at time $t = 0$. For small $\varepsilon \ll 1$ one can write $I(0) \approx (1-k)\varepsilon$. In turn, if two initial values are known at $t = 0$, the basic reproduction number is given by the initial conditions. We prefer to treat the inverse basic reproduction number k and ε as variables, so that $R(0)$ and $I(0)$ are determined by this set. Any other choice of two variables from the set k, ε, $I(0)$, and $R(0)$ would work equally well, as the two remaining ones are then given by Eq. (12).

Preprints (www.preprints.org) | NOT PEER-REVIEWED | Posted: 19 July 2020 doi:10.20944/preprints202007.0416.v1

It it important to realize that the all-time case I has solutions only for a limited range of k values. While there is no recovery when $k = 0$ due to Eq. (7), for $k > 1$ the number of infected would drop (proven below) rather than grow from the boundary value $I(-\infty) = 0$, which is not possible as $I \in [0, 1]$. For $k = 1$, $I(0) = f_1(\varepsilon) = 1 - \varepsilon - e^{-\varepsilon}$ is negative for any $\varepsilon > 0$, and simply remains at its boundary value $I(-\infty) = I(0)$ for $\varepsilon = 0$, and thus $I(t) = 0$ at all times for $k = 1$. Finally, because $I(0) \geq 0$ must hold, not all values in $k \in (0, 1)$ are compatible with the initial condition (11) at time $t = 0$. The requirement $I(0) \geq 0$ is equivalent with $k \leq k_{\max}$ with

$$k_{\max} = \frac{1 - S(0)}{\varepsilon} = 1 - \frac{\varepsilon}{2} + O(\varepsilon^2) \tag{14}$$

This is why the remaining meaningful range of k values is $k \in (0, k_{\max})$ for case I. As the SIR model is assumed to hold at all times, its solution allows to calculate all fractions at times before and after $t = 0$. These two features make case I qualitatively very different from case II.

In contrast, for the semi-time case (B) treated by Kermack and McKendrick[5] and in part B of this work, the SIR model is not assumed to hold at all times, but only at times $t \geq 0$, the time for which feed data may be available. In that case the model cannot be used to calculate fractions at times prior $t = 0$, as this would under many circumstances lead to $S > 1$ or $I \notin [0, 1]$ at times prior to the 'observation' time $t = 0$. Because the boundary conditions of case A must not be respected anymore in that case, one can use arbitrary initial conditions incompatible with Eq. (12). The model in this setup has therefore three independent parameters such as k, $S(0)$ and $I(0)$, while the remaining $R(0)$ is given by Eq. (1). If one chooses the initial conditions to satisfy Eq. (12), we are back at case A. Case B therefore chooses initial conditions incompatible with Eq. (12) such as $S(0) = 1 - \epsilon$ and $I(0) = \epsilon$, implying $R(0) = 0$. In that case one has moreover the freedom to choose $k > 1$, as it does not automatically lead to $I \notin [0, 1]$.

Case B is thus more flexible, but cannot be used to adequately describe the past. While case I can be considered as the solution to the SIR model over the whole time domain, case II can be used to study the future and the case $k > 1$ of relevance towards the end of a epidemics. In this work we are going to study case I and have to thus assume $k \in (0, 1)$ and $\varepsilon \geq 0$.

C. Three important remarks

First, as has been noted before[6], in the three dynamical Eqs. (2), (3) and (6) there is migration from the S-compartment (susceptable) to the I-compartment (infected) at a rate proportional to SI, and removal from the I-compartment to the R-compartment (recovered, dead or isolated) at a rate proportional to I; there is no exit from the R-compartment and no entry into the S-compartment.

Secondly, it is necessary to start initially at time $t = 0$ with at least one infected person, i.e., $I(0) = f_k(\varepsilon) > 0$ (see the second initial condition (12)), as the dynamical Eq. (2) implies for the initial change $\dot{I}(t = 0) = 0$ if $I(t = 0) = 0$. Nothing can grow out of nothing; a situation very similar to kinetic plasma instabilities where seed electromagnetic fluctuations, often from spontaneous emission[23], are needed for starting the instability. Keeping exact tract of the initial conditions during the analysis will prove to be essential to avoid mathematical singularities in the analysis.

Thirdly, the first term on the right-hand side of the dynamical Eq. (2) denotes the newly infected population fraction, i.e., the differential rate of the total fraction $J(t)$ of persons that had ever been infected, i.e.

$$\dot{J}(t) = a(t)S(t)I(t) = -\dot{S}(t), \tag{15}$$

where the second equality results from Eq. (3). It is this rate $\dot{J}(t)$ that can be measured, is usually reported by health agencies along with the cumulative fraction $J(t) = \int_{-\infty}^{t} \dot{J}(\xi)d\xi$, and that has been modeled by the Gaussian time evolution in our earlier work.[3,4] Because $S(0)$, $I(0)$ are usually not reported as they cannot be measured directly, we will show how to replace SIR parameters k and ε by an initial condition for the typically available $J(0)$ and $\dot{J}(0)$.

III. RESULTS

Throughout this work we use the bar-notation $\widetilde{q}$ if we approximate a quantity q.

A. Reduced time

We are here assuming that the infection and recovery rates have the same time dependence, so that their semipositive ratio is time-independent:

$$\frac{\mu(t)}{a(t)} = \frac{\mu_0}{a_0} = k = \frac{1}{R_0} \in [0, 1) \tag{16}$$

corresponding to a basic reproduction number $R_0 > 1$. We emphasize that this special case includes the standard case used by most analysis before that the infection and recovery rates are constants with respect to time. Equation (16) still allows us to take into account an arbitrary time-dependence of the infection rate $a(t)$ which, of course, then is identical to the time dependence of the recovery rate $\mu(t)$ due to assumption (16). Then it is covenient to introduce for arbitrary time dependence of the infection rate $a(t)$ the new dimensionless time variable τ with $\tau(0) = 0$ via

$$\tau(t) = \int_0^t d\xi a(\xi), \tag{17}$$

so that

$$\frac{1}{a(t)}\frac{d}{dt} = \frac{d}{d\tau} \tag{18}$$

Using the reduced time τ, Eqs. (2), (6), and (7) simplify to

$$\frac{d \ln I(\tau)}{d\tau} = S(\tau) - k, \qquad I(\tau) = -\frac{d \ln S(\tau)}{d\tau}, \tag{19}$$

Preprints (www.preprints.org) | NOT PEER-REVIEWED | Posted: 19 July 2020 doi:10.20944/preprints202007.0416.v1

and

$$\frac{dR(\tau)}{d\tau} = kI(\tau) = -\frac{d}{d\tau}[k \ln S(\tau)], \tag{20}$$

respectively. In Eq. (19) $(d \ln S/d\tau)_{\tau=0} = -f_k(\varepsilon)$ in order to meet the initial condition (12) for $I(\tau = 0) = f_k(\varepsilon)$.

Equation (19) includes the well-known threshold[5,6] value k which decides on the so-called J-shape or peak-shape[6] of the pandemic wave. Obviously, Eq. (19) indicates that a peaked pandemic wave cannot emerge if the ratio $k > 1$: as $S \leq 1$ the right-hand side of Eq. (19) in this case is always negative, so that with positive $I(\tau)$ the time derivative $dI/d\tau < 0$, so that the infection rate decreases with time. An epidemic wave emerges if the ratio $k < 1$, corresponding to basic reproduction numbers $R_0 > 1$ greater than unity; the case $k = 1$ we already discussed in Section II B.

The boundary conditions $S(-\infty) = 1$ and $R(-\infty) = 0$ for $t = -\infty$ take over to τ for $k > 0$, because a positive k implies $\mu(t) > 0$ for all t, and thus also $a(t) > 0$ for all t. The solution to Eq. (20) is thus formally equivalent to the relationship we had between $R(t)$ and $S(t)$,

$$R(\tau) = -k \ln S(\tau), \qquad S(\tau) = e^{-\frac{R(\tau)}{k}} \tag{21}$$

B. Analytical solution

Since the original pioneering work[5] the procedure to obtain analytical solutions is similar in later work[6,24] and also here: either (1) one expresses two of the interesting variables $S(t)$, $I(t)$ and $R(t)$ in terms of the third one as done in ref.[5], or (2) one expresses all three variables in terms of a suitable chosen function as done in ref.[24] and here. In both cases one uses Eq. (1) to calculate the solution. Inserting Eqs. (19) and (21), Eq. (1) reads

$$S(\tau) - k \ln S(\tau) - \frac{d \ln S(\tau)}{d\tau} = 1 \tag{22}$$

We emphasize that this equation fulfills the initial conditions (11) for $\tau = 0$. For given rates $a(t)$ and $k = \mu_0/a_0$ the solution of Eq. (22) yields the temporal evolution of $S(t)$. Equation (22) can be written as

$$\frac{d \ln S}{d\tau} = \frac{1}{S}\frac{dS}{d\tau} = S - k \ln S - 1 \tag{23}$$

or

$$\frac{dS/d\tau}{S(S - k \ln S - 1)} = 1, \tag{24}$$

which apart from a different notation corresponds to Eqs. (23) and (27) of Harko et al.[24]. The solution to the dimensional version of Eq. (24) had been expanded into a series $S(t) = \sum_{n=0}^{\infty} a_n t^n$ by Barlow and Weinstein [11], who realized that the convergence radius is rather low and suggested to look for solutions with correct asymptotic behavior, as we'll do here.

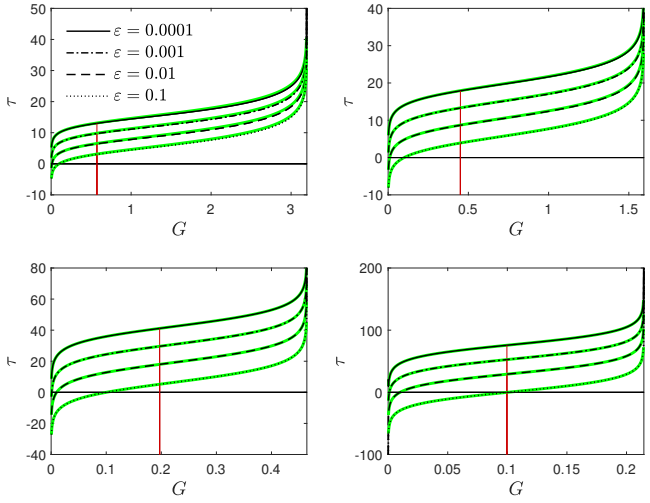

FIG. 1. Exact reduced time τ (black) vs G for (**a**) $k = 0.2$, (**b**) $k = 0.5$, (**c**) $k = 0.8$, and (**d**) $k = 0.9$, according to Eq. (29). Approximant (86) shown in green. The vertical red lines marks $G = G_0$ (54), corresponding to peak time $\tau_0 = \tau(G_0)$. The range of G is given by $G \in [0, G_\infty]$ with G_∞ provided by Eq. (32) or (34).

To this end we follow a slightly different but equivalent approach starting out from Eq. (22). We introduce the quantity $G(\tau)$ by

$$G(\tau) = -\ln S(\tau), \qquad S(\tau) = e^{-G(\tau)} \tag{25}$$

with the initial condition $G(\tau = 0) = \varepsilon$. According to Eqs. (19) and (21) the function G (25) determines

$$R(\tau) = kG(\tau), \qquad I(\tau) = \frac{dG}{d\tau} \tag{26}$$

The dynamical Eq. (22) in terms of $G(\tau)$ reads

$$\frac{dG(\tau)}{d\tau} = 1 - kG(\tau) - e^{-G(\tau)} = f_k[G(\tau)] \tag{27}$$

using the function f_k defined in (13). Integrating

$$\frac{dG/d\tau}{f_k(G)} = 1 \tag{28}$$

over τ then provides (Fig. 1)

$$\tau(G) = \int_\varepsilon^G \frac{dx}{1 - kx - e^{-x}} \tag{29}$$

where the integration constant was determined from the initial condition $G(\tau = 0) = \varepsilon$. The integrand vanishes at $x = 0$ and at certain $x = G_\infty$ to be discussed below. The whole $\tau \in [-\infty, \infty]$ range is thus captured by Eq. (29) upon varying G between zero and G_∞, and vice versa, $G(\tau) \in [0, G_\infty]$ determines the range of G.

The solution (29) generalizes the known analytical solutions in the literature[5,6,24] as it holds for arbitrary time-dependence of the infection rate $a(t)$. The mentioned known

Preprints (www.preprints.org) | NOT PEER-REVIEWED | Posted: 19 July 2020 doi:10.20944/preprints202007.0416.v1

solutions can be reproduced with Eq. (29) by setting $\tau = a_0 t$ on its left-hand side resulting from a constant injection rate a_0. The parametric solution presented in the original SIR work[5] assumed $G \ll 1$ to simplify the analysis. We will see below that $G_\infty \ll 1$ holds only within a very narrow range of k values close to $k = 1$. The contributions within the regime $G \in [0, \varepsilon]$ are usually not considered in numerical schemes while they can be used to verify the proper boundary conditions stated at the very beginning. Harko et al.[24] did show results for $t > 0$ only, as some of the fractions would get negative or exceed unity at times prior $t = 0$, using their analytic solution. We will present an equivalent formulation with $\tau(J)$ of the solution (29) in Eq. (41).

As non-pharmaceutical interventions (NPIs) during the pandemic wave generate a time-changing infection rate $a(t)$, the generalized solution (29) is highly valuable to assess quantitatively the effect of the NPIs on the time evolution of the disease.

C. Maximum value G_∞

The solution (29) indicates that the maximum value $G_\infty = G(\tau = \infty)$ of the function G is attained when the denominator of the integrand vanishes, i.e.

$$f_k(G_\infty) = 0, \tag{30}$$

or

$$e^{-G_\infty} = -k\left(G_\infty - \frac{1}{k}\right) \tag{31}$$

which is of the form (G1) with $c = 1$, $a_0 = -k$ and $r = 1/k$. Consequently, according to Eq. (G2) we obtain (Fig. 2)

$$G_\infty = \frac{1}{k} + W_0(\alpha), \tag{32}$$

where W_0 is the principal solution of Lambert's equation $z = W(z)e^{W(z)}$ (discussed in Appendix G) and α given in terms of k as

$$\alpha = -\frac{e^{-\frac{1}{k}}}{k} \tag{33}$$

The argument α of the Lambert's W_0 function in Eq. (32) is negative for all k (Fig. 15b in Appendix G). Accordingly, $W_0 \in [-1, 0]$ is negative as well (Fig. 15a), while $G_\infty \geq 0$. In Fig. 2 we show the maximum G_∞ as a function of k. It can be seen that G_∞ has values significantly greater than unity for $k \ll 1$, while it vanishes at $k = 1$. The value $G_\infty = 1$ is attained at $k = 1 - 1/e \approx 0.63$. The dashed black line shows the asymptotic behavior of $G_\infty \sim 1/k$ at small $k \ll 1$. Significant deviations from the asymptotic behavior set in at $k \approx 1/3$. According to these considerations, G_∞ is well approximated by (Fig. 2)

$$\widetilde{G}_\infty \simeq \frac{1}{k} - \frac{8k - 1}{7} \tag{34}$$

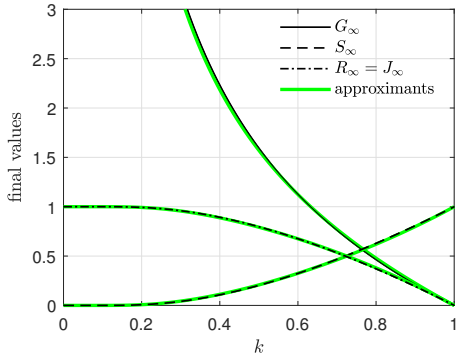

FIG. 2. Analytic final values G_∞, S_∞, R_∞, and J_∞ vs k (black) according to Eqs. (32), (48), and (49), while $I_\infty = 0$ (48). They are all insensitive to the initial conditions. For all these final values, simple approximants (green) based on Eq. (34) are shown as well.

The relative error of this approximant is below 2.2% for $k \leq 0.63$; its absolute error is below 0.014 for $k \geq 0.63$, while it is exact at $k = 1$ and exhibits the correct asymptotic behavior for $k \to 0$.

Similarly, the non-principal solution of Lambert's equation sets the lower bound $G_{-\infty} = G(\tau = -\infty)$ with $G_{-\infty} = k^{-1} + W_{-1}(\alpha) = 0$. The lower bound is identical zero because Lambert's equations is trivially solved by $W_{-1} = -1/k$ for α given by (33). To summarize, $G \in [0, G_\infty]$, compatible with $\tau \in [-\infty, \infty]$ and $S \in [0, 1]$. This compatibility is established as a result of the proper boundary conditions.

D. Differential and cumulative rates of newly infected persons

From the invariant $j(t)dt = j(\tau)d\tau$ we obtain with Eqs. (25), (27), and Eq. (17) in the form $d\tau/dt = a(t)$ for differential rate of newly infected persons from the desease (Fig. 3)

$$j(\tau) = \frac{\dot{J}(t)}{a(t)} = S(\tau)I(\tau) = -\frac{dS(\tau)}{d\tau} \tag{35}$$

$$= f_k(G(\tau))e^{-G(\tau)} \tag{36}$$

with the initial value $j(\tau = 0) = f_k(\varepsilon)e^{-\varepsilon}$. The corresponding cumulative distribution picks up all the newly infected individuals, not only the ones that are going to occur at $t > 0$, i.e., one has (Fig. 4)

$$J(\tau) = \int_{-\infty}^{\tau} d\tau' j(\tau') = -\int_{-\infty}^{\tau} d\tau' \frac{dS(\tau')}{d\tau'}$$

$$= 1 - S(\tau) = 1 - e^{-G(\tau)} \tag{37}$$

In the far past, both quantities j and J emanated from zero, because $G_{-\infty} = 0$. As indicated we may regard these j and J as functions of $G(\tau)$.

Equations (19), (19) in the form $dS/d\tau = -IS$ and $dI/d\tau = SI - kI$ imply with $j = SI$ from Eq. (35)

$$\frac{d\ln j}{d\tau} = S - I - k \tag{38}$$

Preprints (www.preprints.org) | NOT PEER-REVIEWED | Posted: 19 July 2020 doi:10.20944/preprints202007.0416.v1

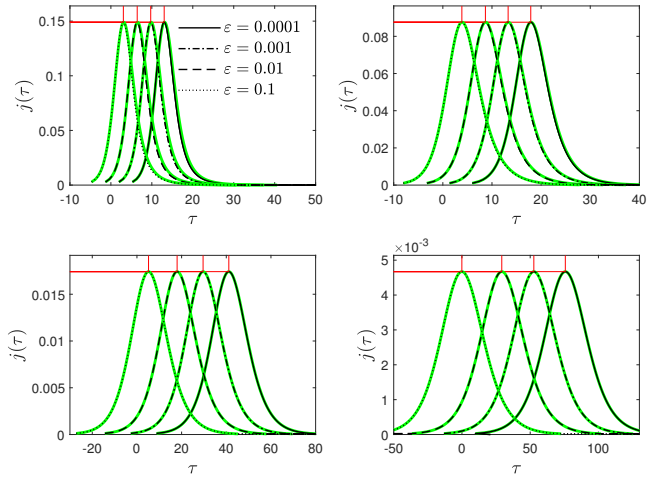

FIG. 3. Differential fraction of infected persons $j(\tau)$ (black) vs reduced time τ for (**a**) $k = 0.2$, (**b**) $k = 0.5$, (**c**) $k = 0.8$, and (**d**) $k = 0.9$, according to Eq. (36). The simple approximant for $j(\tau)$, Eqs. (36) and (86), is shown in green. The peak position, located at τ_0 and $j_{\max}$, is highlighted by vertical and horizontal red lines according to Eqs. (59) and (58). The initial value at $\tau = 0$ is $j(0) = f_k(\varepsilon)e^{-\varepsilon}$, thus different for each k and ε.

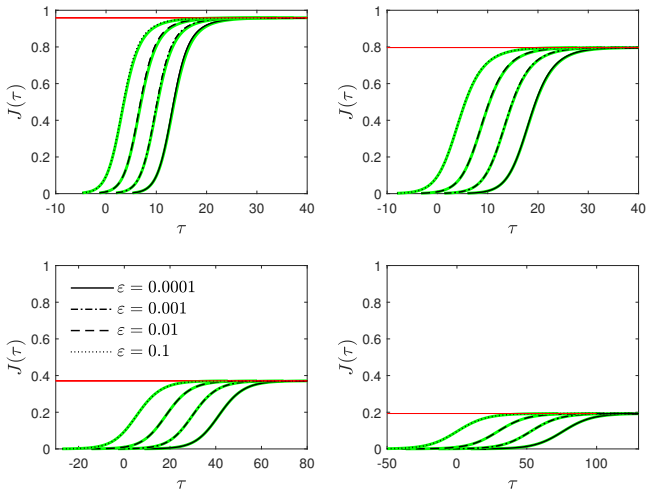

FIG. 4. Cumulative fraction of infected persons $J(\tau)$ (black) vs reduced time τ for (**a**) $k = 0.2$, (**b**) $k = 0.5$, (**c**) $k = 0.8$, and (**d**) $k = 0.9$, according to Eq. (37). Approximants (86) shown in green. The final value is $J_\infty = R_\infty = kG_\infty$ (red) with G_∞ from Eq. (34). Its approximant is given by Eq. (50).

A maximum of $\ln j$ and j thus occurs when $S - I = k$, while (25) and (28) can be used to write $S - I$ in terms of G

$$S - I = 2e^{-G} + kG - 1 \tag{39}$$

Hence Eq. (38) can be written as

$$\frac{d\ln j}{d\tau} = 2e^{-G} + kG - 1 - k \tag{40}$$

Having introduced j and $J = 1 - e^{-G}$, it is worth mentioning that the solution (29) can also be expressed in terms of J as follows. Since $dG/dJ = (1 - J)^{-1}$,

$$\tau(J) = \int_{J(\varepsilon)}^{J} \frac{dy}{(1-y)[y + k\ln(1-y)]} \tag{41}$$

with $J(\varepsilon) = 1 - e^{-\varepsilon}$. The range of J values follows from the range of G values, and is thus given by $J \in [0, J_\infty] = [0, 1 - e^{-G_\infty}] = [0, kG_\infty]$, in light of Eq. (31). With $\tau(J)$ at hand, the remaining quantities of the SIR model are obtained immediately via $S = 1 - J$, $R = -k\ln(1 - J)$, $I = J - R$, and $j = SI$,

E. SIR parameters

The J thus captures all infections up to τ, including those that occurred prior $\tau = 0$, and the usually reported $J(0) = 1 - S(0) = 1 - e^{-\varepsilon}$ provides us with $S(0)$ and ε, i.e.,

$$\varepsilon = -\ln[1 - J(0)] \tag{42}$$

This possibility to determine a parameter does not exist for case II where such quantity J is not available from the model equations and can only be manually entered as a new parameter. Only for case I it is directly related to $S(\tau)$, as we have just shown. Having determined ε from $J(0)$, and assuming $\tau = a_0 t$ with a constant $a_0 = a(t = 0)$, there are two remaining parameters a_0 and k of the SIR model, that we now obtain from the measurable $J(0)$ and its derivatives $\dot{J}(0)$ and $\ddot{J}(0)$ at the initial $t = 0$. To this end we write down expressions for $\dot{J}(0)$ and $\ddot{J}(0)$ and solve them for k and a_0. The first relationship is obtained from $\dot{J}(t) = a_0 j(\tau)$ given by Eq. (36), evaluated at $t = 0$. This yields with $f_k(\varepsilon) = 1 - k\varepsilon - e^{-\varepsilon}$ that

$$k = \frac{1 - e^{-\varepsilon} - \dot{J}(0)e^{\varepsilon}/a_0}{\varepsilon} \tag{43}$$

The second relationship follows from $\ddot{J}(0) = a_0(dj/d\tau)|_{\tau=0}$, using Eqs. (27) and (36). As $dj/d\tau = (dj/dG)f_k(G)$ we can proceed and express $\ddot{J}(0)$ in terms of $G(0) = \varepsilon$, k, and a_0,

$$\begin{aligned}\ddot{J}(0) &= a_0 f_k(\varepsilon)[e^{-\varepsilon} - k - f_k(\varepsilon)]e^{-\varepsilon} \\ &\simeq \varepsilon(1-k)^2 a_0\end{aligned} \tag{44}$$

where the 2nd line can be used if $\varepsilon \ll 1$. Under such conditions

$$\widetilde{a}_0 \simeq \frac{\ddot{J}(0)}{\varepsilon(1-k)^2} \tag{45}$$

Upon replacing k from Eq. (43) in Eq. (45) one can write down an explicit, but lengthy, expression for a_0 in terms of $J(0)$, $\dot{J}(0)$ and $\ddot{J}(0)$. We have thus shown how to obtain all three SIR parameters from the cumulative fraction of newly infected persons J and its derivatives at $t = 0$. In other words, the parameters are obtained from a quadratic fit to the reported $J(t)$, taking into account only data in the vicinity of $t = 0$. Depending on the available data, other expressions presented in this work may be preferred to extract the coefficients, such as Eq. (68).

Preprints (www.preprints.org) | NOT PEER-REVIEWED | Posted: 19 July 2020 doi:10.20944/preprints202007.0416.v1

F. Final values

The knowledge of G_∞ from Eq. (32) and the solution (29) allow us already to derive a number of important results. We first consider the final values at $\tau = \infty$ of (Fig. 2)

$$\begin{aligned} S_\infty &= S(\tau=\infty) = e^{-G_\infty} = 1 - kG_\infty, \\ I_\infty &= I(\tau=\infty) = \frac{dG_\infty}{d\tau} e^{-G_\infty} = 0, \\ R_\infty &= R(\tau=\infty) = k\ln[e^{G_\infty}] = kG_\infty, \end{aligned} \tag{46}$$

where we have used Eqs. (19), (21) and (25). As a consistency check we note that Eq. (1) is fulfilled here, i.e. $S_\infty + R_\infty + I_\infty = 1$. Inserting G_∞ from Eq. (32) we obtain with the help of Eq. (32)

$$R_\infty = 1 + kW_0(\alpha) = kG_\infty \tag{47}$$

$$S_\infty = 1 - R_\infty(k) = -kW_0(\alpha), \tag{48}$$

which both are determined solely by the inverse basic reproduction number $k = 1/R_0$. In Fig. 2 we plot the fractions R_∞ and S_∞ from Eq. (48) as a function of $R_0 > 1$ along with their approximants that follow immediately follow from Eqs. (34) and (46).

If the final values were known, one can calculate the corresponding R_0 upon inverting the relationship between S_∞ and R_0. The result is $R_0 = \ln(S_\infty)/(S_\infty - 1)$. The canonical values $R_\infty = 2/3$ and $S_\infty = 1/3$ are thus reached for $R_0 = 3\ln(3)/2 \approx 1.65$. The final susceptible fraction S_∞ decreases with increasing R_0, starting with $S_\infty = 1$ at $R_0 = 1$, and reaching $S_\infty = 0$ as R_0 grows.

For these values of the differential and cumulative rates of newly infected persons after infinite time we obtain with Eqs. (35) and (46)

$$\begin{aligned} j_\infty &= j(\tau=\infty) = I_\infty S_\infty = 0, \\ J_\infty &= J(\tau=\infty) = 1 - S_\infty = R_\infty = kG_\infty \end{aligned} \tag{49}$$

J_∞ thus coincides with R_∞ (Fig. 2). Its approximant based on Eq. (34) is

$$\widetilde{J}_\infty \approx 1 + \frac{k(1-8k)}{7} \tag{50}$$

With increasing values of k the cumulative fraction of infected persons decreases from 1 at $k = 0$ to 0 at $k = 1$.

G. Bell-shaped differential rate. GM-like solution of the SIR

Equation (36) can also be used, even without the explicit inversion of Eq. (29), to derive generally valid expressions for the time τ_0 of maximum, the maximum level $j_{\max}$ and the dimensionless width ω of the differential rate j, which correspond to the three important parameters characterizing a Gaussian differential rate,

$$j(\tau) = j_{\max} e^{-\frac{(\tau-\tau_0)^2}{\omega^2}} \tag{51}$$

although here the width ω may not be a τ-independent constant. Assuming a constant ω, Eq. (51) is known as the Gauss model (GM) for the time evolution of the daily number of new infections (or also deaths).[4]

a. Exact peak amplitude The maximum of the differential rate (36) occurs when the derivative $dj/d\tau$ in Eq. (40) vanishes providing

$$2e^{-G_0} + kG_0 = 1 + k \tag{52}$$

directly from Eqs. (38) and (39). Writing this as

$$e^{-G_0} = -\frac{k}{2}\left(G_0 - \frac{1+k}{k}\right) \tag{53}$$

makes the equation of the form (G1) with $c = 1$, $a_0 = -k/2$ and $r = (1+k)/k$. The analytic solution of Eq. (52) is the non-principal solution W_{-1} of Lambert's equation ,

$$G_0 = \frac{1+k}{k} + W_{-1}(\alpha_0), \qquad \alpha_0 = \frac{2\alpha}{e} \tag{54}$$

with α from (33). If W in (54) were the principal solution W_0 of Lambert's equation, with the property $W_0(\alpha) \in [-1, 0]$ and $W_0(\alpha_0) \in [-0.406, 0]$ for $k \in [0, 1]$ (Appendix G), then $G_0 = G_\infty + 1 + W_0(\alpha_0) - W_0(\alpha)$ would exceed G_∞. The W in (54) is therefore the non-principal solution W_{-1} of Lambert's equation with the property $W_{-1}(\alpha_0) \le -2$ for all $k \in [0, 1]$, as shown in Appendix G. A simple approximant for G_0 is

$$\widetilde{G}_0 \simeq (1-k)\left(1 + \frac{5}{9}k\right)\ln 2 \tag{55}$$

It is exact at $k = 0$ and $k = 1$ and has a maximum absolute error of 0.008.

Inserting Eq. (52) in Eq. (36) yields an analytic expression for the maximum value

$$j_{\max} = j(G_0) = \left(e^{-G_0} - k\right)e^{-G_0} \tag{56}$$

$$= \frac{k^2}{4}\left\{[1 + W_{-1}(\alpha_0)]^2 - 1\right\} \tag{57}$$

$$= \frac{(1-kG_0)^2 - k^2}{4} \tag{58}$$

where the 1st, 2nd, and 3rd line are obtained with the help of (36), (54), (53), respectively. Since $W_{-1}(\alpha_0) \le -2$ for all $k \in [0, 1]$, the $j_{\max}$ positive. For $k = 1$ the $W_{-1}(\alpha_0) = -2$ and $j_{\max}$ vanishes. For $k \to 0$ the $W_{-1}(\alpha_0)$ diverges to $-\infty$ (Appendix G), but the k^2 in front causes $j_{\max}$ to approach $1/4$. Note that $j_{\max}$ (58) is not affected by ε but solely determined by the inverse basic reproduction number k. This is reflected by the results shown in Fig. 3: regardless of ε the maximum value $j_{\max}$ remains unchanged for given k. A simple approximant for $j_{\max}$ is provided by Eq. (77).

We recall that the maximum $j_{\max}$ in the measurable daily number of new infections is completely different from the maximum population fraction $I_{\max}$ of the infected compartment. Because $I(\tau) = f_k(G)$ it achieves its maximum at $I_{\max} = 1 - k + k\ln k$ according to Eq. (A2).

b. Peak time The time, at which $j_{\max}$ is reached, must not be positive. The maximum may have occurred already, depending on the initial condition and the value for the inverse basic reproduction number k. According to solution (29) the

Preprints (www.preprints.org) | NOT PEER-REVIEWED | Posted: 19 July 2020 doi:10.20944/preprints202007.0416.v1

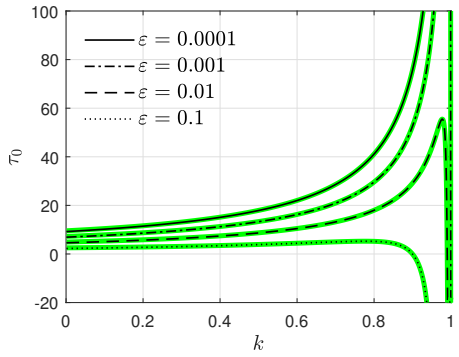

FIG. 5. Dimensionless peak time of daily infections, τ_0 vs. k for various ε. Exact solution (solid black) compared with the analytic approximant τ_0 (green) from Eq. (59). The peak time in real units is τ_0/a_0, and corresponds to the number of days between the time of maximum daily infections and the time for which initial conditions have been specified. Because $G_0(k=1)=0$, depending on the initial condition characterized by ε, the τ_0 becomes negative for sufficiently large k (the peak time has already passed).

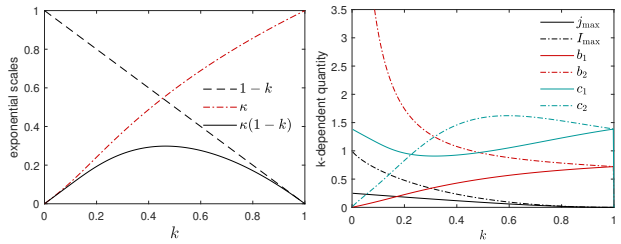

FIG. 6. (**a**) Quantities $1-k$, κ defined by Eq. (61) as well as $\kappa(1-k)$, where $1-k$ and $\kappa(1-k)$ characterize the exponential increase and decay of the differential rate j at early and late times. By determining k from the regime of exponential growth at early times, the exponential decrease at late times is already encoded in $\kappa(1-k)$. (**b**) Several k-dependent quantities entering the approximant $\widetilde{G}(\tau)$, such as $b_{1,2}$ and $c_{1,2}$ required in Eq. (87). Also shown is the exact maximum differential rate of newly infected, $j_{\max}$, and maximum fraction of the infected compartment, $I_{\max}$.

value of $G_0(k)$ corresponds to the time of maximum $\tau_0(k)$ where G_0 and τ are given by Eqs. (54) and (29). An explicit expression for τ_0 in terms of k and ε is given upon inserting G_0 from Eq. (54) into Eq. (86). This yields (Fig. 5)

$$\tau_0 = \tau(G_0) = \frac{A(\varepsilon) - A(G_0)}{\kappa(1-k)} \tag{59}$$

with the very useful abbreviations

$$A(x) = \ln\left(1 - \frac{x}{G_\infty}\right) + \ln\left(\frac{G_\infty}{x}\right)^\kappa \tag{60}$$

and (Fig. 6a)

$$\kappa = \frac{k[1 + W_0(\alpha)]}{1-k} \tag{61}$$

where $1 + W_0(\alpha)$ is identical with the crossover x^* from Eq. (A11). We can use this κ with the feature $\kappa \in (0,1)$ to rewrite

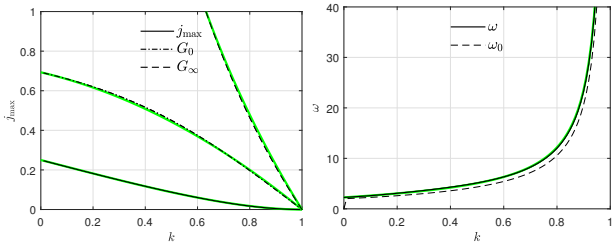

FIG. 7. Analytic results (black) for the (**a**) amplitude $j_{\max}$ and (**b**) widths of the differential rate $j(\tau)$ vs. k according to Eqs. (58), (74) and (66). Also shown in (A): G_0 (54) and G_∞ for comparison with G_0. For all exact results, the simple approximants (34), (55), (76) and (77) are shown for comparison in green.

the exact expression (32) as

$$G_\infty = \frac{(1-k)(1+\kappa)}{k} \tag{62}$$

Figure 3 indicates that the peak time τ_0 varies inversely with ε, confirming Eq. (59).

c. Exact behavior in the vicinity of the maximum With the help of Eqs. (28) and (40) one has

$$\frac{d^2 \ln j}{d\tau^2} = f_k(G)\frac{d \ln j}{dG} = (k - 2e^{-G}) f_k(G) \tag{63}$$

so that a 2nd order Taylor expansion of $\ln j(\tau)$ around its maximum

$$\ln j(\tau) = \ln j_{\max} + \frac{(\tau-\tau_0)^2}{2}\left.\frac{d^2 \ln j}{d\tau^2}\right|_{\tau=\tau_0} + O(\tau-\tau_0)^3 \tag{64}$$

can be evaluated, where $\ln j_{\max}$ is given by Eq. (58). Making use of e^{-G_0} as given by (53), Eq. (63) evaluated at $\tau = \tau_0$, or equally, $G = G_0$, simplifies to

$$\left.\frac{d^2 \ln j}{d\tau^2}\right|_{\tau=\tau_0} = -\frac{2}{\omega_0^2} \tag{65}$$

with (Fig. 7b)

$$\omega_0 = \frac{2}{\sqrt{(1-kG_0)(1-kG_0-k)}} \tag{66}$$

We thus have for the Taylor expansion of $\ln j(\tau)$ around its maximum value at τ_0 to second order, $\ln j(\tau) = \ln j_T(\tau) + O(\tau-\tau_0)^3$ with

$$\ln j_T(\tau) = \ln j_{\max} - \frac{(\tau-\tau_0)^2}{\omega_0^2} \tag{67}$$

with ω_0 given by Eq. (66).

d. Exact asymptotic behavior of the SIR model Next we show that the rate $j(\tau)$ exhibits exponential behavior at early and late times with respect to the peak time and evaluate the growth coefficients.

Making use of the limiting values $G(\tau=-\infty)=0$ and $G(\tau=\infty)=G_\infty$ in Eq. (40) we find the growth coefficients

Preprints (www.preprints.org) | NOT PEER-REVIEWED | Posted: 19 July 2020 doi:10.20944/preprints202007.0416.v1

characterizing exponential growth and decrease at early and late times,

$$\lim_{\tau\to-\infty} j(\tau) = j_{\text{early}} e^{(1-k)(\tau-\tau_0)}, \tag{68}$$

$$\lim_{\tau\to+\infty} j(\tau) = j_{\text{late}} e^{-\kappa(1-k)(\tau-\tau_0)} \tag{69}$$

with κ from Eq. (61) and τ_0 from Eq. (59). Note that the exponent in (68) is positive, and the exponent in (69) is negative since $\kappa > 0$ for all $k \in (0, 1)$.

To calculate the important prefactors in these expressions we start from Eq. (B2). At small times, where $g = G/G_\infty$ approaches zero, we use the Taylor expansion $\ln(1-g) = -g$ to obtain

$$G(\tau) \simeq \kappa G_0 W_0\left[\frac{e^{(1-k)\tau + A(\varepsilon)/\kappa}}{\kappa}\right] \tag{70}$$

for $g \ll 1$ as the solution of Eq. (B2). Since the argument of Lambert's principal solution W_0 gets small in this limit, cf. Eq. (G10), because $j = (1-k)G + O(G^2)$, and with the help of τ_0 (59) and $A(x)$ (60) we obtain for the regime of early times $\tau \ll \tau_0$

$$\begin{aligned} j_{\text{early}} &= (1-k)G_\infty e^{-A(G_0)/\kappa} \\ &= (1-k)G_0\left(1 - \frac{G_0}{G_\infty}\right)^{-1/\kappa} \end{aligned} \tag{71}$$

In the opposite limit, where $g = G/G_\infty$ approaches unity, we can use the Taylor expansion $\ln(g) = g - 1 + O(1-g)^2$ to obtain

$$G(\tau) \simeq G_\infty\left\{1 - W_0\left[\frac{e^{-\kappa(1-k)} e^{A(\varepsilon)}}{\kappa}\right]\right\} \tag{72}$$

for $1 - g \ll 1$ as the solution of Eq. (B2). Since the argument of Lambert's function W gets again small in this limit, because $j = \kappa(1-k)(G - G_\infty)e^{-G_\infty} + O[(G_\infty - G)^2]$, we obtain for the regime at late times $\tau \gg \tau_0$

$$\begin{aligned} j_{\text{late}} &= \kappa(1-k)G_\infty e^{-G_\infty} e^{A(G_0)} \\ &= \kappa(1-k)(G_\infty - G_0)\left(\frac{G_\infty}{G_0}\right)^{\kappa} e^{-G_\infty} \end{aligned} \tag{73}$$

We have thus shown that the initial condition $S(0)$ enters only the peak time τ_0 and the that prefactors j_{early} and j_{late} characterizing the amplitudes of the asymptotic behaviors depend on k alone. Their dependency on k is shown in Fig. 8. While j_{early} reaches its maximum at $k \to 0$, where the SIR reproduces the SI model (section F), j_{late} becomes very small in this limit. As a matter of fact, the asymptotic behavior of the SI model, corresponding to a value unity in Fig. 8, is all that can be observed up to huge times $\tau \sim k^{-1}$ (denoted as τ_c in Appendix F), as not only the prefactor j_{late} becomes extremely small in the limit $k \to 0$, but also the contribution $j_{\text{late}}/\kappa(1-k)$ from the asymptotic exponential to the cumulative J.

These expressions (68), (69), (71) and (73) exactly capture the short and long time behavior of $j(\tau)$ shown in Fig. 3. The coefficients ε and k can thus also be read off from the regime of exponential growth, if a_0 is already known. It is worthwhile noticing that the initial condition $S(0)$ does only affect the peak time, but not the prefactors j_{early} and j_{late} in the asymptotic behavior of j.

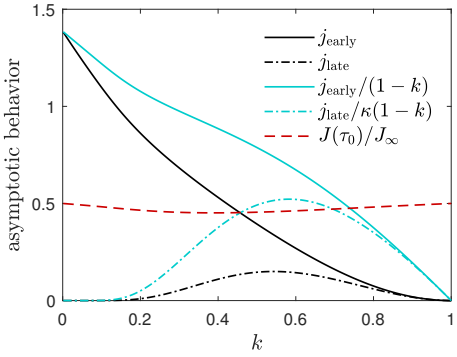

FIG. 8. Quantities j_{early} (71) and j_{late} (73) versus k characterize the magnitude of the asymptotic exponential increase and decay of the differential rate j. Also shown are the hypothetical contributions to the cumulative J if j were fully captured by its asymptotes, evaluated at early and late times. The actual contribution from times prior peak time τ_0 to the cumulative J is $J(\tau_0)/J_\infty = (1 - e^{-G_0})/kG_\infty$ (shown as well). For the symmetric GM and the logistic model this fraction is $1/2$.

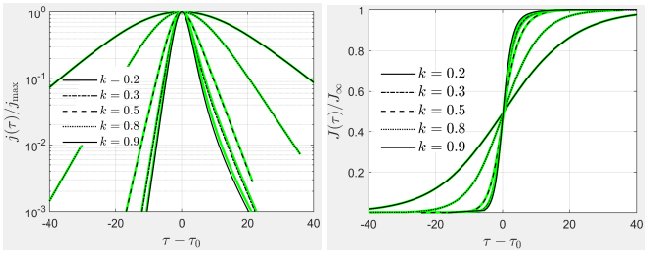

FIG. 9. SIR model (**a**) reduced differential $j(\tau)/j_{\max}$ and (**b**) reduced cumulative fraction $J(\tau)/J_\infty$ of infected persons versus time relative to peak time, $\tau - \tau_0$, according to Eqs. (36) and (37), with τ_0 from (59), for various k. Approximant (86) shown in green. The asymptotic behaviors of the differential j at small and large τ are in full agreement with our analytic expressions (68) and (69) with (71) and (73).

e. Gaussian width While j is not a perfect gaussian, as it is not perfectly symmetric (to be discussed below), we can calculate a width via three routes. Route (A) fits $j(\tau)$ by the gaussian function (51) with constant w. Route (B) determines w by the known GM relationship $w = J_\infty/\sqrt{\pi} j_{\max}$ using our above results for J_∞ and $j_{\max}$. The third route is to estimate a width from the behavior in the vicinity of the peak times. The latter leads to width ω_0 (66). The former two routes give rise to very compatible widths ω as function of k (all widths shown in Fig. 7b).

Making use of our above results (49), (46), (32), we can thus express a τ-independent characteristic width of $j(\tau)$ analytically as

$$\omega = \frac{4G_\infty}{\sqrt{\pi}k\{[1 + W_{-1}(\alpha_0)]^2 - 1\}} \tag{74}$$

$$= \frac{4G_\infty}{\sqrt{\pi}k[(G_0 - k^{-1})^2 - 1]} \tag{75}$$

where $\alpha_0 = 2\alpha/e$ and α expressed in terms of k in (33), and where we have used G_0 from Eq. (54). Note, that also the

Preprints (www.preprints.org) | NOT PEER-REVIEWED | Posted: 19 July 2020 doi:10.20944/preprints202007.0416.v1

width is not affected by ε, but solely determined by the inverse basic reproduction number k. Taking into account all limiting behaviors our approximant for ω is given by

$$\widetilde{\omega} \approx \frac{4+2k(1-k)}{\sqrt{\pi}(1-k)} \tag{76}$$

implying, with the help of our approximant $\widetilde{G}_\infty$ (34)

$$\widetilde{j}_{\max} = \frac{k\widetilde{G}_\infty}{\sqrt{\pi}\widetilde{\omega}} \approx \frac{(1-k)^2(7+8k)}{14(2-k)(1+k)} \tag{77}$$

Both are compared with the exact results in Fig. 7. The two frequencies ω_0 and ω are actually very comparable which lead us to the GM-like approximant to be discussed next. We recall that the dimensional $\hat{j}_{\max} = a_0 j_{\max}$ for a constant $a(t)$, and that the dimensional width is then $w = \omega/a_0$.

f. GM-like approximant for $j(\tau)$ We have by now calculated the behavior of $\ln j(\tau)$ around its maximum including peak height (denoted as $j_T(\tau)$ in Eq. (67)), and the asymptotic behavior of $j(\tau)$ at small and large τ. Using a continuity requirement we can construct an approximant $\widetilde{j}(\tau)$ for $j(\tau)$ that captures the behavior of $j(\tau)$ qualitatively at all times. The continuity requirement is, in light of Eqs. (68), (69),

$$\ln j_T(\tau_{\text{early}}) = \ln j_{\text{early}} + (1-k)(\tau_{\text{early}} - \tau_0), \tag{78}$$

$$\ln j_T(\tau_{\text{late}}) = \ln j_{\text{late}} - \kappa(1-k)(\tau_{\text{late}} - \tau_0) \tag{79}$$

where j_{early} and j_{late} are given by Eqs. (71), (73), and where the two times τ_{early} and τ_{late} have to be determined by the continuity conditions. The condition (78), with $j_T(\tau)$ from Eq. (67), yields

$$\tau_{\text{early}} = \tau_0 - \frac{1}{2}(1-k)(1+D_{\text{early}})\omega_0^2, \tag{80}$$

$$D_{\text{early}} = \sqrt{1 + \frac{4\ln(j_{\max}/j_{\text{early}})}{(1-k)^2\omega_0^2}} \tag{81}$$

Similarly, condition (79) yields

$$\tau_{\text{late}} = \tau_0 + \frac{1}{2}\kappa(1-k)(1+D_{\text{late}})\omega_0^2, \tag{82}$$

$$D_{\text{late}} = \sqrt{1 + \frac{4(\ln(j_{\max}/j_{\text{late}}))}{\kappa^2(1-k)^2\omega_0^2}} \tag{83}$$

The full GM-like approximant for $j(\tau)$ therefore reads (Fig. 10)

$$\widetilde{j}_{\text{GML}}(\tau) = \begin{cases} j_{\text{early}} e^{(1-k)(\tau-\tau_0)}, & \tau \le \tau_{\text{early}} \\ j_{\max} e^{-(\tau-\tau_0)^2/\omega_0^2}, & \tau \in [\tau_{\text{early}}, \tau_{\text{late}}] \\ j_{\text{late}} e^{-\kappa(1-k)(\tau-\tau_0)}, & \tau \ge \tau_{\text{late}} \end{cases} \tag{84}$$

with j_{early} and j_{late} given by Eqs. (71), (73), κ defined by Eq. (61), τ_{late} and τ_{late} according to Eqs. (80), (82), ω_0 specified by Eq. (66), and τ_0 denoting the peak time $\tau_0 = \tau(G_0)$ from Eq. (59) or Eq. (59). The classical GM[4] is a special case of the GM-like approximant for $\tau_{\text{early}} = -\infty$ and $\tau_{\text{late}} \to \infty$.

Not under all conditions the central gaussian part meets the asymptotic exponential tails. Both D_{early} and D_{late} can get complex-valued as soon as the argument of the square root gets negative. This is the case for D_{late} if τ_0 is sufficiently large negative. Under such conditions the relevant crossover times are the real parts of τ_{early} and τ_{late}, and the asymptotic branches are only shown up to the level that is reached by $j_T(\tau)$.

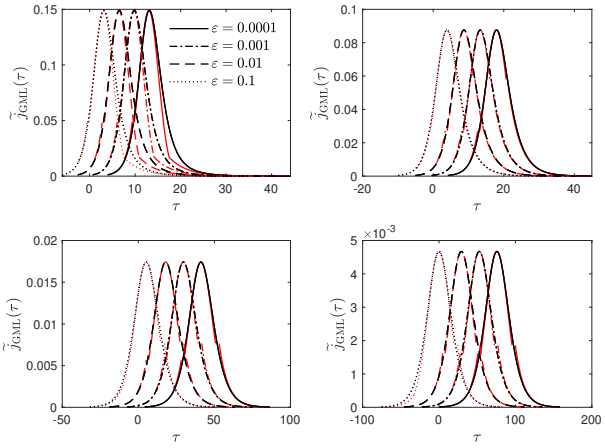

FIG. 10. Comparison of the GM-like approximant given by Eq. (84) (red) and the numerically exact $j(\tau)$ (black). The GM-like approximant has three regimes, divided by characteristic times τ_{early} and τ_{late}, where the asymptotic exponential behavior turns into a gaussian-shaped time-evolution that captures the j in the neighborhood of the peak time. The GM is especially useful prior the climax of the epidemy, where is had been used to estimate the GM parameters. We have shown here how to map these parameters to the parameters of the corresponding SIR model.

Our GM-like approximant (84) suggests that the GM is a suitable approximation for times between τ_{early} and τ_{late}. The ω from Eq. (74) and ω_0 from Eq. (66) are found to be very similar, which implies that J_∞ calculated for the GM can serve as an estimate for the exact J_∞, as done in Ref.[4]. The difference between the GM and the SIR can also be visualized by eliminating time, and plotting $j/j_{\max}$ versus J/J_∞ (Fig. 11).

The value of τ_{early} can be most easily determined from the differential and cumulative doubling times[25] of the GML-approximant (84), as both are constants below t_{early}. t_{early} coincides with the time when the monitored doubling times start to increase with time.

Similarly, τ_{late} can be determined when the differential decay time (although this is seldomly reported) or the cumulative doubling time become constants at late times of a pandemic wave.

The cumulative

$$\widetilde{J}_{\text{GML}}(\tau) = \int_{-\infty}^{\tau} \widetilde{j}_{\text{GML}}(\tau')d\tau' \tag{85}$$

as well as the final $\widetilde{J}_\infty$ corresponding to the GM-like $\widetilde{j}(\tau)$ then follow by integration. Analytic expressions are provided in Appendix H.

Preprints (www.preprints.org) | NOT PEER-REVIEWED | Posted: 19 July 2020 doi:10.20944/preprints202007.0416.v1

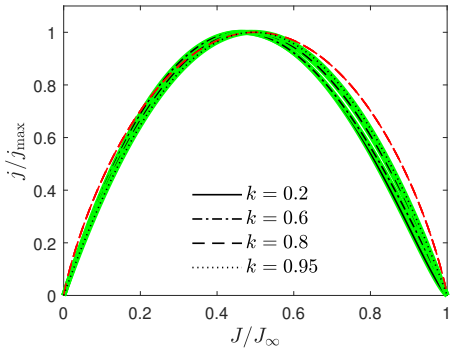

FIG. 11. Reduced differential rate $j/j_{\max}$ versus reduced cumulative rate $J/J - \infty$. This representation of the result eliminates time, and thus τ_0. Shown are results of the SIR model for various k (black) together with our approximants $\widetilde{\tau}(G)$ and $\widetilde{G}(\tau)$ (green, both identical in this representation), and the simple GM (red) for comparison. The larger k, the better the simple GM (red) captures the SIR. The GM is especially useful prior the climax of the epidemy, where is had been used to estimate the GM parameters.[4]

IV. FURTHER REDUCTION OF SOLUTION (29)

In order to derive explicit analytical expressions $G(\tau)$ it is necessary to calculate, at least approximately, the remaining integral on the right-hand side of Eq. (29). Whereas in the references[6,24] the analytical evaluation of this remaining integral is not detailed, we recall that in the pioneering work[5] this was done for small values of G less than unity by expanding the exponential function in the denominator to second order in x about $x = 0$, i.e. $e^{-x} \simeq 1 - x + x^2/2$. However, this approximation cannot be applied here for all values of G as Fig. 2 indicates that G_∞ attains values significantly greater than unity. Therefore more generally, without referring to the regime $x \ll 1$, an analytic approximant $\widetilde{\tau}$ for τ can be derived, as shown in Appendix A

$$\widetilde{\tau}(G) = \frac{1}{1-k}\left[\ln(G/\varepsilon) + \frac{1}{\kappa}\ln\frac{G_\infty - \varepsilon}{G_\infty - G}\right] \qquad (86)$$

that is valid for all $k \in (0,1)$ and all $\varepsilon \ll 1$. The κ was defined in terms of k by Eq. (61). We note that Eq. (86) can alternatively be written as $\widetilde{\tau}(G) = [A(\varepsilon) - A(G)]/\kappa(1-k)$ with A defined by Eq. (60). Obviously, $\widetilde{\tau}(G = \varepsilon) = 0$ is fulfilled for this approximant. Upon replacing G by G_0 in (86), we arrive at the expression (59) for the peak time. In Fig. 1 we compared the numerically evaluated integral (29) with the approximation (86) for various k. We notice the excellent agreement.

Even more important in practise, we were able to invert the relationship (86) to obtain an approximant $\widetilde{G}(\tau)$. This is done in Appendix (B). There we use this approximant to confirm that it exhibits correct asymptotic behaviors, that it reproduces the exact $j_{\max}$, and shares the peak time τ_0 with $\widetilde{\tau}(G)$ exactly. To be specific we obtain

$$\frac{\widetilde{G}(\tau)}{G_\infty} = \begin{cases} b_1 W_0[c_1 e^{(1-k)(\tau-\tau_0)}], & \tau \le \tau_0 \\ 1 - b_2 W_0[c_2 e^{-\kappa(1-k)(\tau-\tau_0)}], & \tau \ge \tau_0 \end{cases} \qquad (87)$$

where the k-dependent parameters $b_{1,2}$ and $c_{1,2}$ (Fig. 6b) are specified in Appendix B, τ_0 given by Eq. (59), and W_0 is the principal solution of Lambert's equation (Appendix G). With $\widetilde{G}(\tau)$ at hand, one can express all results in terms of τ, and thus also in terms of time t – for arbitrary $a(t)$ – without preparing a parametric plot. The approximant (87) is implemented in the Supplementary Material (Appendix I).

V. TIME-DEPENDENT INFECTION RATE $a(t)$

As we have demonstrated, J_∞ and all other final values are insensitive to the precise time-dependency of $a(t)$. It is possible to flatten the curve of daily infections $\dot{J}_{\max} = a(t_0) j_{\max}$ by interventions that reduce $a(t_0)$ at peak time t_0 given by $\tau_0 = \tau(t_0)$. Here $\dot{J}_{\max}$ is the maximum population fraction that is newly infected within a single day, if we choose day as the time unit in which we also express the infection rate $a(t)$.

While $J(t) = J(\tau)$ is invariant, the differential rates are related as $\dot{J}(t) = \dot{\tau} j(\tau) = a(t) j(\tau(t))$. Inserting $\tau(t)$ for an arbitrarily chosen $a(t)$ into the expression for $j = f_k(G)e^{-G}$ with $G = \widetilde{G}(\tau)$ from Eq. (87), the daily number of new infections is available analytically as function of time.

Starting from Eqs. (36) and (37) one has $G = -\ln(1-J)$ and $S = 1 - J$, so that we can write down a relationship between differential $j(\tau)$ and cumulative $J(\tau)$ number of infected persons,

$$j = (1-J)[J + k\ln(1-J)] \qquad (88)$$

The same relationship follows from the derivative of Eq. (41) with respect to τ. Since $j(\tau) = a(t)\dot{J}(t)$, the infection rate $a(t)$ can be extracted from the measured $\dot{J}(t)$ and $J(t)$ via the right hand side of Eq. (88), divided by $\dot{J}(t)$, as long as k is time-independent.

VI. SUMMARY AND CONCLUSIONS

We demonstrated that the exact parametric solution $S(t)$, $I(t)$ and $R(t)$ to the SIR model with time-dependent $a(t)$, time-independent k and arbitrary initial conditions is determined by the function $G(\tau)$ uniquely specified Eq. (29). The t-dependency of G is given by $\tau(t)$ from Eq. (17). With $G_t = G(\tau(t))$ as function of t therefore at hand,

$$S(t) = e^{-G_t}, \qquad R(t) = kG_t, \qquad (89)$$

and $I(t) = 1 - S(t) - R(t)$ solve the SIR equations at all times, and satisfy the boundary and initial conditions exactly. The measurable differential rate of newly infected $\dot{J}$ and its cumulative counterpart J are then available from $\dot{J}(G_t) = a(t)S(t)I(t)$ and $J(G_t) = 1 - S(t)$, according to Eqs. (36) and (37). Alternatively, one can go over the $J(\tau)$ route instead of $G(\tau)$ as explained in section III D.

While the SIR model is usually solved numerically, and the relationship between G and τ given by Eq. (29) can also be calculated numerically, we provide analytic approximants

Preprints (www.preprints.org) | NOT PEER-REVIEWED | Posted: 19 July 2020 doi:10.20944/preprints202007.0416.v1

$\widetilde{G}(\tau)$ (87) as well as for the inverse $\widetilde{\tau}(G)$ (86) both have the correct asymptotic behaviors and may be use instead of the exact result, as they are sufficiently accurate for any practical purpose. Using this approximant (87), that works for any k and any initial condition, the usually reported daily number of new infections we have expressed explicitly as function of time t for an arbitrarily time-dependent infection rate $a(t)$ in section V. The presented solution of the all-time SIR model can thus be used to replace the numerical solution of the SIR model. Having an analytical solution should be also advantageous to understand the effect of interventions reflected by $a(t)$ much easier, and in a more transparent fashion.

The whole shape of the differential rate j depends on k only. The shape is characterized by the maximum $j_{\max}$ (58), width ω (74), asymptotic exponents $1-k$ and $-\kappa(1-k)$ as well as their prefactors j_{early} (71) and j_{late} (73), while the initial condition affects the peak time τ_0 (59). All these quantities have been determined analytically in this work for the all-time SIR model. In addition, we have provided approximants for all quantities characterizing the exact solution of the SIR model, to appreciate their qualitative behavior, or in case the Lambert functions are unavailable. For the special case of time-independent $a(t) = a_0$, and thus $\tau = a_0 t$, the SIR parameters k, ε, and a_0 can all be determined from initial conditions $J(0)$, $\dot{J}(0)$, and $\ddot{J}(0)$ by Eqs. (42), (43), (45). This is important because the I and R fractions are usually not reported at a certain time to provide an initial condition.

Our derivation not only generalizes existing solutions, but may appear very compact compared with existing ones, while it includes them as a special case. We have relaxed the assumptions of $t \geq 0$ and $G \ll 1$ from previous approaches, and present the unique solution that captures consistently both the future and the past, if the SIR model is assumed to hold in the past as well. The classical assumption $G \ll 1$ we have shown to fail except at inverse basic reproduction numbers close to unity.

The evolution of the usually reported differential rates assumes a bell-shaped curve characterized by a peak time τ_0, height $j_{\max}$, and width ω. We have provided analytic expressions for all these parameters by Eqs. (59), (58), and (74), respectively. They involve the two solutions W_0 and W_{-1} of Lambert's equation, usually available in scientific software. To appreciate the validity of our arguments and derivations, we have collected the required exact features of W_0 and W_{-1} in Appendix G.

We have inspected the limiting case of $k \to 0$ of the SIR model to find that the SI model, corresponding to $k = 0$, does not trivially emerge from the SIR model in this limit. While the asymptotic behavior of the SIR model is qualitatively different from the SI model, the quantitative difference between them still decreases with decreasing k. Insofar is the SI model compatible with the limiting case of an SIR model, but at the same time asymptotically different.

The semi-time SIR model, which can be considered as the SIR model subject to initial conditions incompatible with the all-time SIR model, and thus useful to predict only the future time-evolution, will be elaborated in part B of this work.

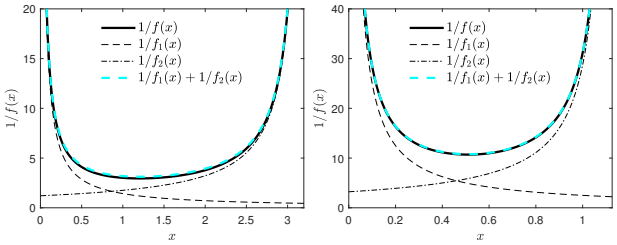

FIG. 12. Integrand $1/f(x)$ with $f(x)$ defined by (A1) for (a) $k = 0.3$ ($G_\infty \approx 3.20$) and (b) $k = 0.6$ ($G_\infty \approx 1.13$) (black). The asymptotic behavior is captured at small x by $1/h_1(x)$ (dashed gray) and at large x by $1/h_2(x)$ (dashed gray). Our approximant (A5) (yellow) appears to basically coincide with the integrand, and has the correct asymptotic behavior by construction.

Appendix A: Approximant $\widetilde{\tau}(G)$ for $\tau(G)$

Here we address the formal solution (29)

$$\tau = \int_\varepsilon^G \frac{dx}{f_k(x)}, \tag{A1}$$

with f_k defined in (13), over the range of all possible values for $G \in [0, G_\infty]$ and $k \in [0,1]$, where G_∞ is given by (32). For the special case of $G = G_0$, we thus also address the peak time $\tau_0 = \tau(G_0)$ introduced in Section III G. The f_k in the denominator of the integral is semipositive, has its maximum at $x_m = -\ln(k)$, and reaches zero at G_∞. A 2nd root of f_k is located at $x = 0$. Accordingly, f_k has the following properties: $f_k(0) = f_k(G_\infty) = 0$, $f_k'(0) = 1-k$, $f_k'(x_m) = 0$, and

$$f_k^{\max} = f_k(x_m) = 1 - k + k \ln k, \tag{A2}$$

For $x \ll 1$ the function $f_k(x)$ can be expanded about $x = 0$ as $f_k(x) = h_1(x) + \mathcal{O}(x^2)$ with

$$h_1(x) = (1-k)x \tag{A3}$$

Likewise, for large x we expand f_k about G_∞ to obtain $f_k(x) = h_2(x) + \mathcal{O}((G_\infty - x)^2)$ with

$$\begin{aligned} h_2(x) &= (x - G_\infty)[1 - k(1 + G_\infty)] \\ &= \kappa(1-k)(G_\infty - x) \end{aligned} \tag{A4}$$

with κ from equation (61). Using these asymptotes we obtain the following approximant

$$\frac{1}{f_k(x)} = \frac{1}{h_1(x)} + \frac{1}{h_2(x)} \tag{A5}$$

Examples for the cases of $k = 0.3$ and $k = 0.6$ are shown in Fig. 12. Both partial integrals can be performed analytically as

$$\tau_1(G) = \int_\varepsilon^G \frac{dx}{h_1(x)} = \frac{\ln(G/\varepsilon)}{1-k}, \tag{A6}$$

$$\tau_2(G) = \int_\varepsilon^G \frac{dx}{h_2(x)} = \frac{1}{\kappa(1-k)} \ln\left[\frac{G_\infty - \varepsilon}{G_\infty - G}\right] \tag{A7}$$

Preprints (www.preprints.org) | NOT PEER-REVIEWED | Posted: 19 July 2020 doi:10.20944/preprints202007.0416.v1

and $\widetilde{\tau}(G) = \tau_1(G) + \tau_2(G)$. While τ_1 dominates the integral at small G, at $G = \varepsilon$ and beyond, τ_2 is responsible for the sharp increase at large G, when G approaches G_∞ (see Fig. 1). With $A(x)$ defined by Eq. (60), $\widetilde{\tau}(G)$ can alternatively be written as

$$\widetilde{\tau}(G) = \frac{A(\varepsilon) - A(G)}{\kappa(1-k)} \tag{A8}$$

The exact asymptotic behaviors at small and large G are

$$\lim_{G\to 0} \tau(G) = \lim_{G\to 0} \tau_1(G) = -\infty, \tag{A9}$$

$$\lim_{G\to G_\infty} \tau(G) = \frac{\ln(G_\infty/\varepsilon)}{1-k} + \lim_{G\to G_\infty} \tau_2(G) = \infty \tag{A10}$$

where the intermediate expressions are also required, e.g., to calculate j_{late} in Eq. (73).

As already noted, $h_1(x)$ and $h_2(x)$ dominate the behavior of the integrand in distinct x regimes. To specify the regimes, we solve $h_1(x^*) = h_2(x^*)$ to obtain

$$x^* = 1 + W_0(\alpha) = \frac{\kappa(1-k)}{k} \tag{A11}$$

with the help of (32), and where we recall that $W_0(\alpha) \in [-1, 0)$ is negative for all $k \in [0, 1]$. For $x < x^*$ the dominating contribution is $h_1(x)$. While $x^* = 1$ for $k = 0$ and $x^* \approx 1$ for $k < 0.2$, it depends almost linearly on k for larger k and reaches $x^* = 0$ for $k = 1$. From Eq. (A6) we infer

$$G(\tau) \approx \varepsilon e^{(1-k)\tau}, \qquad G \ll x^* \tag{A12}$$

and G_0 given by Eq. (54) we can derive from equation (A11) the inequality

$$G_0 \le x^* \tag{A13}$$

for all k, while $G_0 = x^*$ at $k = 1$ follows from the mentioned properties of Lambert's functions.

Appendix B: Approximant $\widetilde{G}(\tau)$ for $G(\tau)$

Starting from the high quality approximant $\widetilde{\tau}(G)$ derived in the foregoing section, we are looking for an explicit expression for the inverse function, $\widetilde{G}(\tau)$. Unfortunately, $\widetilde{\tau}(G)$ cannot be inverted analytically over the whole G domain, but we are going to find approximants for G separately over the two disjunct intervals $\widetilde{G} \in [0, G_0]$ and $\widetilde{G} \in [G_0, G_\infty]$ so that

$$\frac{\widetilde{G}(\tau)}{G_\infty} = \begin{cases} g_1(\tau), & \tau \le \tau_0 \\ g_2(\tau), & \tau \ge \tau_0 \end{cases} \tag{B1}$$

with g_1, g_2 given in terms of k and ε by equations (B4), (B6) to be derived in this section, and compared with the exact $G(\tau)$ in Fig. 13. We recall that G_∞ is known in terms of k by Eq. (32). The two partial approximants meet exactly at $\tau = \tau_0$ specified by Eq. (59).

To derive all quantities appearing in equation (B1) we start from $\widetilde{\tau} = \tau_1 + \tau_2$ in terms of G, provided by equations (A6) and (A7). Upon introducing $g = G/G_\infty$ and the known $g_0 = G_0/G_\infty$, using the abbreviation κ already introduced by equation (61), the governing equation for g is written

$$\kappa \ln g - \ln(1-g) = \kappa(1-k)\tau - A(\varepsilon) \tag{B2}$$

involving the g-independent and semipositive constant $A(\varepsilon)$ defined by Eq. (60). Equation (B2) leads to the exact transcendental equation

$$\frac{g^\kappa}{1-g} = e^{\kappa(1-k)\tau - A(\varepsilon)} \tag{B3}$$

that cannot be solved analytically. To proceed we approximate, for the two cases of $g > g_0$ and $g < g_0$ separately, corresponding to $\tau \le \tau_0$ and $\tau \ge \tau_0$, respectively, the smaller of the two logarithmic terms. In each case we make sure that the approximation is correct in all limiting cases, so that not only the asymptotic behavior of G and j will be correctly captured, but also g_1 and g_2 will coincide at $\tau = \tau_0$.

a. Approximant $\widetilde{G}_1(\tau) = g_1(\tau)G_\infty$. To obtain g_1 we approximate $\ln(1-g) \simeq -C_1 g$ in equation (B2) with a constant C_1 in such a way that the approximation is exact at both $g = 0$ and $g = g_0$. This yields $C_1 = -g_0^{-1}\ln(1-g_0)$. If we furthermore introduce x via $g = e^{-x}$, the corresponding equation for x is of the form (G1) with $c = 1$, $r = A(\varepsilon)/\kappa - (1-k)\tau$, and $a_0 = \kappa/C_1$. Its solution is thus $x = r + W_0(e^{-r}/a_0)$, involving W_0 and not W_{-1} because the argument $e^{-r}/a_0 \ge 0$ (Fig. 15). With x at hand, we have found $g_1 = \ln x$ which can be written with the help of Lambert's equation in two equivalent ways

$$g_1(\tau) = b_1 W_0(c_1 x_1) = \frac{W_0(c_1 x_1)}{W_0(c_1)} g_0, \tag{B4}$$

both for a different purpose. In equation (B4) we have introduced the abbreviations $b_1 = \kappa/C_1 = -\kappa g_0/\ln(1-g_0)$,

$$c_1 = -\frac{\ln(1-g_0)}{\kappa(1-g_0)^{1/\kappa}}, \qquad x_1 = e^{(1-k)(\tau-\tau_0)} \tag{B5}$$

with $g_0 = G_0/G_\infty$, so that x_1 carries the dependency on time, and is unity at $\tau = \tau_0$ with τ_0 according to (59). G_0, κ and A explicitly given by Eqs. (54), (61), and (60). This expression for τ_0 is just another way of writing the expression (59) for τ_0 we obtained from $\widetilde{\tau}(G)$ in the previous section. The equivalence follows already from Eq. (B2). The right hand side of Eq. (B4) proves that $g_1(\tau_0) = g_0$.

b. Approximant $\widetilde{G}_2(\tau) = g_2(\tau)G_\infty$. For the opposite case of large g close to unity. we use the same strategy as before and now approximate $\ln(g) \simeq C_2(g-1)$ with a constant C_2 in such a way that the approximation is exact at both $g = 1$ and $g = g_0$. This yields $C_2 = -(1-g_0)^{-1}\ln g_0$. If we proceed in a way analogous to the case of g_1, we obtain

$$g_2(\tau) = 1 - b_2 W_0(c_2 x_2) = 1 - \frac{W_0(c_2 x_2)}{W_0(c_2)}(1-g_0), \tag{B6}$$

Here we have introduced the abbreviations $b_2 = (\kappa C_2)^{-1} = (g_0 - 1)(\kappa \ln g_0)^{-1}$,

$$c_2 = -\frac{\kappa \ln g_0}{g_0^\kappa}, \qquad x_2 = e^{-\kappa(1-k)(\tau-\tau_0)} \tag{B7}$$

Preprints (www.preprints.org) | NOT PEER-REVIEWED | Posted: 19 July 2020 doi:10.20944/preprints202007.0416.v1

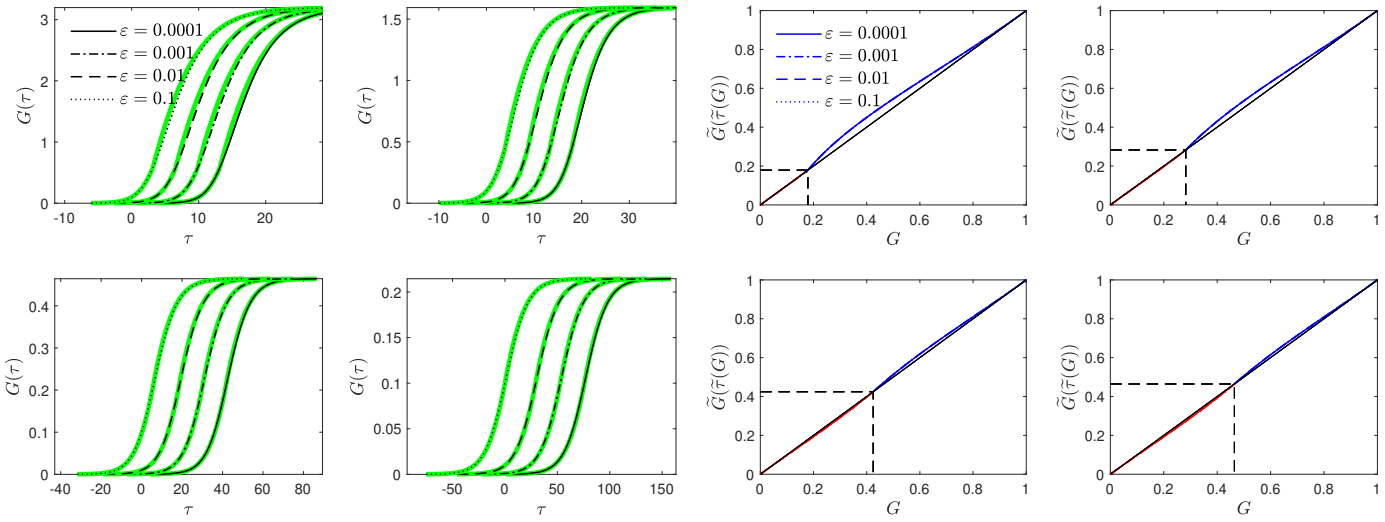

FIG. 13. Comparison of the numerically exact $G(\tau)$ (black) with the approximant $\widetilde{G}(\tau)$ from Eqs. (B1) (green) versus k for various ε (black).

FIG. 14. Comparison of the two approximants $\widetilde{\tau}(G)$ and $\widetilde{G}(\tau)$. Shown is $\widetilde{G}(\widetilde{\tau}(G))$ versus G, where the part with $G \le G_0$ is colored red, while the remaining part is blue. The dashed lines marks the point (G_0, G_0), and the black line is a guide for the eye. The approximants are inverse to each other independent on the value of ε. All these curves fall on top of each other.

so that x_2 carries the dependency on time, is unity at $\tau = \tau_0$, where τ_0 was already given by Eq. (59) or (59).

The two half approximants (B4) and (B6) (Fig. 13) perfectly match at G_0 by construction, i.e., by the proper choice of the approximants for $\ln(1-y)$ and $\ln y$. The calculations leading to the present form of the approximants had to make use of properties of Lambert's function, in particular the identity $W(z \ln z) = \ln z$ (G6) for any positive z. Note that the dependency of $\widetilde{G}(\tau)$ on ε is adsorbed by x_1 and x_2, while all other coefficients are positive and depend on k only. The coefficients are not independent of each other, as

$$b_2 c_2 = (b_1 c_1)^{-\kappa} = \frac{1-g_0}{g_0^\kappa} \tag{B8}$$

holds. To summarize, in this section we have provided an explicit expression for the approximant $\widetilde{G}(\tau)$ in terms of k and ε, and also an approximant for the peak time τ_0 in terms of the same parameters. Because the assumptions were asymptotically exact, the approximant has the features

$$\begin{aligned} \lim_{\tau\to-\infty} \widetilde{G}(\tau) = G_\infty \lim_{x_1\to 0} g_1(\tau) = \lim_{x_1\to 0} b_1 c_1 x_1 = 0, \\ \lim_{\tau\to\infty} \widetilde{G}(\tau) = \lim_{x_2\to 0} G_\infty (1 - b_2 c_2 x_2) = G_\infty, \end{aligned} \tag{B9}$$

as expected, and $\widetilde{G}(\tau)$ is compared with the exact $G(\tau)$ in Fig. 13. To arrive at Eq. (B9), we used property (G10) of the Lambert's function. Approximants $\widetilde{\tau}(G)$ and $\widetilde{G}(\tau)$ are compared with each other in Fig. 14.

Appendix C: Approximant $\widetilde{S}(\tau)$ for $S(\tau)$

$S(\tau)$ had been defined by equation (25). Using the identity $W(z) = \ln(z) - \ln W(z) = \ln[z/W(z)]$ implies $aW(z) = \ln[z/W(z)]^a$ and $e^{-aW(z)} = [W(z)/z]^a$. We thus have, starting from the result of the previous section,

$$\widetilde{S}_1(\tau) = e^{-\widetilde{G}_1(\tau)} \simeq \left[\frac{W_0(c_1 x_1)}{c_1 x_1}\right]^{b_1 G_\infty}, \tag{C1}$$

$$\widetilde{S}_2(\tau) = e^{-\widetilde{G}_2(\tau)} \simeq \left[\frac{W_0(c_2 x_2)}{c_2 x_2}\right]^{-b_2 G_\infty} e^{-G_\infty} \tag{C2}$$

where $\widetilde{S}_1(\tau)$ captures the regime before, and $\widetilde{S}_2(\tau)$ the regime after the peak time τ_0. As these approximants have correct asymptotic behavior, the exact asymptotic behavior of $S(\tau)$ follows from these expressions with Eq. (G10).

Appendix D: Approximants $\widetilde{I}(\tau)$ and $\widetilde{R}(\tau)$

Since $R = kG$ according to Eqs. (26) and $S + I + R = 1$, we can write immediately down our approximants for $R(\tau)$ and $I(\tau)$

$$\widetilde{R}(\tau) = k\widetilde{G}(\tau), \tag{D1}$$

$$\widetilde{I}(\tau) = 1 - \widetilde{S}(\tau) - k\widetilde{G}(\tau) \tag{D2}$$

$$= 1 - k\widetilde{G}(\tau) - e^{-\widetilde{G}(\tau)} \tag{D3}$$

with $\widetilde{G}$ and $\widetilde{S}$ given by Eqs. (B1) and (C2).

Appendix E: Approximant $\widetilde{j}(\tau)$ for $j(\tau)$

The differential rate $j(\tau)$ had been defined by equation (35) or the equivalent equation (36). With $\widetilde{G}(\tau)$ from Eq. (B1) at

Preprints (www.preprints.org) | NOT PEER-REVIEWED | Posted: 19 July 2020 doi:10.20944/preprints202007.0416.v1

hand we can calculate the approximant for $\widetilde{j}(\tau)$ via equation (36).

$$\widetilde{j}(\tau) = \widetilde{I}(\tau)\widetilde{S}(\tau) \simeq \begin{cases} j_1(\tau), & \tau \leq \tau_0 \\ j_2(\tau), & \tau \geq \tau_0 \end{cases} \tag{E1}$$

with τ_0 according to equation (59) or Eq. (59). with the approximants for $\widetilde{I}(\tau)$ and $\widetilde{S}(\tau)$ in terms of $\widetilde{G}$ already written down in Eqs. (D3), (C1), and (C2). Obviously, j_1 meets j_2 at $\tau = \tau_0$, because $G_1(\tau_0) = G_2(\tau_0)$. Note that this is not the case if Eq. (35) is used, as the slopes of $\widetilde{S}_1$ and $\widetilde{S}_2$ are not exactly identical at $\tau = \tau_0$. The prefactors of this approximant in the asymptotic limits of early and late times differ from the exact Eqs. (71), (73) only by a factor C_1 and C_2, respectively, introduced in section B. Both factors approach unity for small ε, and start to deviate from unity only at large $\varepsilon \gtrsim 0.2$.

The maximum of the approximant coincides with the exact $j_{\max}$, because we have determined $\widetilde{j}$ using Eq. (36), and because the definition of G_0 implies $j_{\max} = (e^{-G_0} - k)e^{-G_0}$, which remains unchanged, as the maximum of the approximant occurs at $\tau = \tau_0$, where $G = G_0$.

1. Remark: Non-monotonous $d\widetilde{S}/d\tau$

If we calculate the approximant $\widetilde{j}(\tau)$ starting from Eq. (35), using the notation from Appendix B, with $dx_1/d\tau = (1-k)x_1$, and the property (G8) of Lambert's function, this gives

$$\begin{aligned} \widetilde{j}_1(\tau) &= -\frac{d\widetilde{S}_1}{d\tau} = -\frac{c_1 dx_1}{d\tau}\frac{dS_1}{d(c_1x_1)} \\ &= \frac{(1-k)G_\infty}{[1+W_0(c_1x_1)]} g_1(\tau)\widetilde{S}_1(\tau) \end{aligned} \tag{E2}$$

Similarly, with $dx_2/d\tau = -\kappa(1-k)x_2$,

$$\begin{aligned} \widetilde{j}_2(\tau) &= -\frac{d\widetilde{S}_2}{d\tau} = -\frac{c_2 dx_2}{d\tau}\frac{dS_2}{d(c_2x_2)} \\ &= \frac{\kappa(1-k)G_\infty}{[1+W_0(c_2x_2)]}[1-g_2(\tau)]\widetilde{S}_2(\tau) \end{aligned} \tag{E3}$$

At $\tau = \tau_0$, these expressions simplify with $x_1 = x_2 = 1$, $g_1(\tau_0) = g_2(\tau_0) = g_0$, $\widetilde{S}_1(\tau_0) = \widetilde{S}_2(\tau_0)$. We thus have

$$\begin{aligned} \frac{\widetilde{j}_1(\tau_0)}{\widetilde{j}_2(\tau_0)} &= \frac{(1-k)g_0}{[1+W_0(c_1)]}\frac{[1+W_0(c_2)]}{\kappa(1-k)(1-g_0)} \\ &= \frac{1}{\kappa}\frac{[1+W_0(c_2)]}{[1+W_0(c_1)]} \end{aligned} \tag{E4}$$

If we now make use of relationships from Appendix B, i.e., replace $W_0(c_1) = -\kappa^{-1}\ln(1-g_0)$, $W_0(c_2) = -\kappa \ln g_0$, and κ by its definition (61), we see that this ratio is unity for a single k, but not all $k \in (0,1)$. This is because $d\widetilde{S}/d\tau$ is generally non-monotonic.

Appendix F: The case of vanishing k

For the extremal case of $k = 0$ (so-called SI model), which is shown here to emerge nontrivially from the SIR model in the limit $k \to 0$, the differential equation (27) for $G(\tau)$ with $G(0) = \varepsilon$ is solved by

$$G_{\rm SI}(\tau) = \ln(1 + e^{\tau - \tau_0^{\rm SI}}), \qquad \tau_{\rm SI}^0 = -\ln(e^\varepsilon - 1) \tag{F1}$$

hence $S_{\rm SI}(\tau) = e^{-G_{\rm SI}(\tau)} = 1 - J_{\rm SI}(\tau) = [1 + e^{\tau - \tau_{\rm SI}^0}]^{-1}$ and

$$I_{\rm SI}(\tau) = 1 - S_{\rm SI}(\tau) = \frac{e^{\tau - \tau_{\rm SI}^0}}{1 + e^{\tau - \tau_{\rm SI}^0}} \tag{F2}$$

since $R_{\rm SI} = 0$ at all times for $k = 0$. The differential rate is given by $G_{\rm SI}(\tau)$ via Eq. (36) or via Eq. (35), or from $dJ_{\rm SI}/d\tau$, as

$$j_{\rm SI}(\tau) = \frac{e^{\tau - \tau_{\rm SI}^0}}{(1 + e^{\tau - \tau_{\rm SI}^0})^2} \tag{F3}$$

The same result is obtained with $j_{\rm SI}(\tau) = I_{\rm SI}(\tau)S_{\rm SI}(\tau)$ using the solution of the logistic equation, mentioned in Section (II B). Its maximum with amplitude $j_{\rm SI}^{\max} = 1/4$ thus occurs at $\tau_{\rm SI}^0$, the asymptotic behavior is given by $\lim_{\tau\to-\infty} j_{\rm SI}(\tau) = e^{\tau - \tau_{\rm SI}^0}$ and $\lim_{\tau\to\infty} j_{\rm SI}(\tau) = e^{-(\tau - \tau_{\rm SI}^0)}$, and the GM-like behavior in the vicinity of $\tau = \tau_{\rm SI}^0$ follows from the Taylor-expansion as $j_{\rm SI}(\tau) \simeq [1 - (\tau - \tau_{\rm SI}^0)^2]/4$, corresponding to $\omega_0 = 2$. Within the SI model, every person gets infected in the course of time, $J_{\rm SI}^\infty = 1$, but nobody will ever get uninfected again (through recovery/removal).

Importantly, while some quantities like $G_{\rm SI}^\infty = \infty$, $G_{\rm SI}^0 = \ln(2)$, $j_{\rm SI}^{\max} = 1/4$ obviously agree with the values one obtains for the SIR in the limit $k \to 0$, the exponential decay of $j_{\rm SI}$ (F3) of the logistic SI model ($k = 0$) is qualitatively different from the SIR model at times after peak time, as the SIR exponent $-\kappa(1-k)$ tends to reach zero for $k \to 0$. In fact, the deviations between SI and the $k \to 0$ limit of the SIR get smaller with decreasing k. This can be seen by inspecting τ in the regime where it is large, and G close to G_∞. For small k one has $\kappa \simeq k$ and $\kappa(1-k) \approx k$, as well as $G_\infty \simeq k^{-1}$ and thus, according to Eq. (A7),

$$\tau \simeq \tau_2 \simeq \frac{1}{k}\ln\left(\frac{1-k\varepsilon}{1-kG}\right) \simeq -\frac{1}{k}\ln(1-kG) \tag{F4}$$

as k approaches zero. This relationship can be inverted to write $G \simeq k^{-1}(1 - e^{-k\tau})$. Since $e^{-k\tau} = 1 - k\tau + O(k^2)$ for any finite τ, the G approaches τ, and j thus approaches, albeit very slowly with decreasing k, the limiting $e^{-(\tau-\tau_0)}$, in agreement with the SI model (F3). To be more precise, the SIR approaches the SI in the sense

$$\lim_{k\to 0}\int_{-\infty}^{\infty}[j(\tau) - j_{\rm SI}(\tau)]^2\, d\tau = 0 \tag{F5}$$

while for any small but finite k, the SIR j still enters the regime $j \propto e^{-\kappa(1-k)\tau} \simeq e^{-k\tau}$ at some finite crossover

Preprints (www.preprints.org) | NOT PEER-REVIEWED | Posted: 19 July 2020 doi:10.20944/preprints202007.0416.v1

$\tau = \tau_c < \infty$ that can be estimated by equating this asymptotics with Eq. (F3). The asymptotics of the SIR at large times is thus different from the SI, but the numerical difference between the SI and SIR results still decreases with decreasing k. To estimate τ_c in the limit of small k, one can safely use the mentioned approximations $G_\infty \simeq k^{-1}$ and $\kappa(1-k) \simeq k$. By equating the two differential rates (69) with (73) and (F3) the governing equation for he crossover τ_c is thus $e^{-1/k}(k\varepsilon)^{-k}e^{-k\tau_c} = e^{-\tau_c}/(e^\varepsilon - 1)$, or equivalently,

$$\tau_c \simeq \frac{1}{k} + k\ln(k\varepsilon) - \ln(e^\varepsilon - 1) \tag{F6}$$

where we have used another relationship, $k(1-k) \simeq k$, also valid for small k. Further assuming $k \ll \varepsilon \ll 1$, this latter expression simplifies to

$$\tau_c \simeq \frac{1}{k} - \ln(\varepsilon) \tag{F7}$$

The crossover τ_c thus increases not only strongly with decreasing k but moreover slowly with decreasing ε, and this makes Eq. (F5) to hold.

Another signature of qualitatively different setting between the SI and SIR at $k \to 0$ is the relationship $J_\infty = R_\infty$ for the SIR, which breaks down at $k = 0$, as R does not depend on time for $k = 0$, and thus $R_{\rm SI}^\infty = 0$ and $I_{\rm SI}^\infty = 1$, while the limiting behavior of the SIR model is $\lim_{k\to 0} R = \lim_{k\to 0} kG_\infty = 1$.

Irrespective these observations, for an arbitrary infection rate $a(t)$, the daily number of new infections as function of time t is given for the SI model by Eq. (F3) with $\tau = \int_0^t a(t')dt'$.

Appendix G: Lambert's equation. Solutions and their properties

Lambert's W function[26,27] with several applications in physics[28–33] solves the equation $z = W(z)e^{W(z)}$. It can be used to calculate the solution of transcendental equations of the form

$$e^{-cx} = a_0(x - r) \tag{G1}$$

in explicit form as

$$x = r + \frac{1}{c}W\left(\frac{ce^{-cr}}{a_0}\right) \tag{G2}$$

The two real-valued solutions are denoted by W_0 (principal) and W_{-1} (non-principal) as shown by Fig. 15a. These two functions are available in scientific software such as `lambertw` (Matlab$^{\rm R}$) or `ProductLog` (Mathematica$^{\rm R}$).

For the purpose of this manuscript we are interested in $W(\alpha)$ and $W(\alpha_0)$ as function of $k \in [0,1]$, where $\alpha = -e^{-1/k}/k$ (32) and $\alpha_0 = 2\alpha/e$ (54). The two α's and their ranges are depicted as function of k in Fig. 15b. While $\alpha \in [-e^{-1}, 0]$ for any k, the $\alpha_0 \in [-2e^{-2}, 0]$. The lower bound is in each case reached at $k = 1$. One has $W_0(0) = 0$,

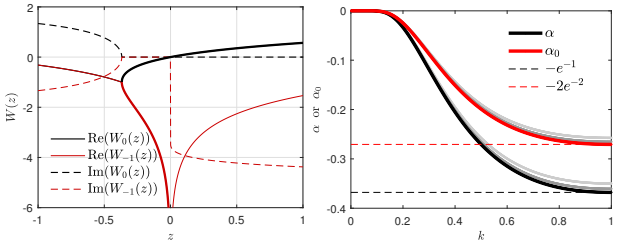

FIG. 15. (**a**) Principal W_0 and non-principal W_{-1} solutions of Lambert's equation $z = W(z)e^{W(z)}$. As can be seen, there is single real-valued solution for $z \geq 0$, and two real-valued solutions for $z \in [-1/e, 0]$. Complex-valued solutions are represented by thin lines. The thick black line is the real-valued $W_0(z) \in [-1, 0]$ for $z \geq -1/e$, while the thick red line is the real-valued $W_{-1}(z) \leq -1$ for $z \in [-1/e, 0]$. (**b**) α and α_0 vs k for $\varepsilon = 0$ (thick), $\varepsilon = 0.02$ and $\varepsilon = 0.05$ (thin). One has $\alpha \geq -e^{-1} \approx -0.368$ and $\alpha_0 \geq -2e^{-2} \approx -0.271$ for all $k \in [0, 1]$ and $\varepsilon \geq 0$.

$W_{-1}(0) = -\infty$, $W(-e^{-1}) = -1$, $W_0(-2e^{-2}) \approx -0.406$, and $W_{-1}(-2e^{-2}) = -2$ as one can verify by pluggin in these values into Lambert's equation. Accordingly, for the case of α the solutions of Lambert's equation reside in the disjunct ranges $W_0(\alpha) \in [-1, 0]$ and $W_{-1}(\alpha) \in [-\infty, -1]$. For α_0 the solutions reside in the disjunct ranges $W_0(\alpha_0) \in [-0.406, 0]$ and $W_{-1}(\alpha_0) \in [-\infty, -2]$. These ranges are used to select the relevant solutions of Lambert's equation in (32) and (54). A special, trivial but important case is $z = -e^{-1/k}/k = \alpha(\varepsilon = 0)$ because this z obviously solves Lambert's equation exactly with the simple $W_{-1}(z) = -k^{-1}$, i.e., one has

$$W_{-1}\left(-\frac{e^{-1/k}}{k}\right) = -\frac{1}{k} \tag{G3}$$

for all k. Using the same α's, Lambert's W functions have the following property

$$W_0(\alpha) - W_{-1}(\alpha_0) \geq 1 \tag{G4}$$

that implies $G_0 \leq G_\infty$. Proof. As is obvious from Fig. 15b, the difference between α and α_0 is largest at $k = 1$ and $\varepsilon = 0$. For these special values $W_0(\alpha) = W_0(-e^{-1}) = -1$ and $W_{-1}(\alpha_0) = W_{-1}(2e^{-2}) = -2$. The difference then changes monotonously and becomes huge in the limit $k \to 0$ (and $\alpha \to 0$), as is obvious from Fig. 15b. This completes the proof.

Another important inequality is

$$W_{-1}(\alpha) - W_{-1}(\alpha_0) \leq 1 \tag{G5}$$

as it implies $G_0 \geq G_{-\infty} = 0$. Proof. The left hand side increases with increasing k, as $\alpha - \alpha_0$ increases as well (Fig. 15b). At $k = 1$, $W_{-1}(\alpha) = W_{-1}(-e^{-1}) = -1$ and $W_{-1}(\alpha_0) = W_{-1}(-2e^{-2}) = -2$. This completes the proof.

There is another identity that we need to derive the final expression for our approximant $\widetilde{G}(\tau)$.

$$W\left(z\ln z\right) = \ln z \tag{G6}$$

Preprints (www.preprints.org) | NOT PEER-REVIEWED | Posted: 19 July 2020 doi:10.20944/preprints202007.0416.v1

holds for any $z > 0$. As a proof one can start from this expression for W, to obtain $We^W = (\ln z)e^{\ln z} = z \ln z$, which is Lambert's equation. A function W with the property (G6) fulfills Lambert's equation at the same time, as long as W is real-valued; equation (G6) is thus equivalent to Lambert's equation over the domain of positive arguments.

Taking the derivative of Lambert's equation $z = We^W$ with respect to z, Lambert's functions W_0 and W_{-1} both obey the differential equation

$$z\frac{dW}{dz} = \frac{W(z)}{1+W(z)} \tag{G7}$$

so that

$$x\frac{dW(cx)}{dx} = \frac{W(cx)}{1+W(cx)}, \tag{G8}$$

$$x\frac{dW(cx)}{dx} - W(cx) = -\frac{W^2(cx)}{1+W(cx)} \tag{G9}$$

Relationships (G8) and (G9) are required if one attempts calculating the approximant $\widetilde{j}$ from $-d\widetilde{S}/d\tau$.

For small z, Lambert's function W_0 has the expansion

$$W_0(z) = z - z^2 + \frac{3}{2}z^3 + O(z^4) \tag{G10}$$

implying

$$\frac{W_0(z)}{z} = 1 - z + \frac{3}{2}z^2 + O(z^3), \tag{G11}$$

$$\frac{W_0(z)}{1+W_0(z)} = z - \frac{z^3}{2} + O(z^4) \tag{G12}$$

Appendix H: Cumulative $\widetilde{J}(\tau)$ for GM-like solution of the SIR

The cumulative $\widetilde{J}_{\rm GML}(\tau) = \int_{-\infty}^{\tau} \widetilde{j}_{\rm GML}(\tau')d\tau'$ corresponding to $\widetilde{j}_{\rm GML}(\tau)$ given by the GM-like Eq. (84) follows by integration. One has

$$\widetilde{J}_{\rm GML}(\tau) = \begin{cases} \widetilde{J}_1(\tau), & \tau \le \tau_{\rm early}, \\ \widetilde{J}_1(\tau_{\rm early}) + \widetilde{J}_T(\tau), & \tau \in [\tau_{\rm early}, \tau_{\rm late}] \\ \widetilde{J}_1(\tau_{\rm early}) + \widetilde{J}_T(\tau_{\rm late}) + \widetilde{J}_2(\tau), & \tau \ge \tau_{\rm late} \end{cases} \tag{H1}$$

with

$$\widetilde{J}_1(\tau) = \frac{j_{\rm early}e^{(1-k)(\tau-\tau_0)}}{1-k},$$

$$\widetilde{J}_T(\tau) = \frac{j_{\rm max}\omega_0\sqrt{\pi}}{2}\left[\mathrm{erf}\left(\frac{\tau-\tau_0}{\omega_0}\right) + \mathrm{erf}\left(\frac{\tau_0-\tau_{\rm early}}{\omega_0}\right)\right],$$

$$\widetilde{J}_2(\tau) = \frac{j_{\rm late}\left[e^{-\kappa(1-k)(\tau_{\rm late}-\tau_0)} - e^{-\kappa(1-k)(\tau-\tau_0)}\right]}{\kappa(1-k)} \tag{H2}$$

Appendix I: Supplementary: Implementation

For the convenience of a reader, this section contains a complete Mathematica™ notebook that creates time-dependent SIR results using our $\widetilde{G}(\tau)$ for an arbitrary infection rate a[t], specified in the first line, arbitrary $k \in (0, k_{\rm max})$ and $S(0) \in (0,1)$. All results such as $S(t)$ (code SIRS[k,S0][t]) and $\dot{J}(t)$ (code SIRj(k,S0][t]) are available analytically, and can be plotted as shown.

```
a[t_] := 1;
tau[t_] = Integrate[a[s], {s, 0, t}];

W[type_, x_]:= ProductLog[type, x];
W0[k_]:= W[0, -Exp[-1/k]/k];
W1[k_]:= W[-1, -2 Exp[-1/k - 1]/k];
kp[k_]:= k (1 + W0[k])/(1 - k);
pk[k_]:= 1/kp[k];
f[k_][x_]:= 1 - k x - Exp[-x];
Gf[k_]:= 1/k + W0[k];
G0[k_]:= (1+k)/k + W1[k];
A[k_][x_]:=Log[(1-x/Gf[k])Power[Gf[k]/x,kp[k]]];
Ae[k_,S0_]:= A[k][-Log[S0]];
A0[k_]:= A[k][G0[k]];
jmax[k_]:=((1-k G0[k])^2-k^2)/4;
Jf[k_]:=k Gf[k];
tau0[k_,S0_]:=(Ae[k,S0]-A0[k])/(kp[k](1-k));

(* approximant G[tau] *)
g0[k_]:= G0[k]/Gf[k];
b1[k_]:= -kp[k] g0[k]/Log[1 - g0[k]];
b2[k_]:= (g0[k] - 1)/(kp[k]Log[g0[k]]);
c1[k_]:= -Log[1-g0[k]]/(kp[k]Power[1-g0[k],pk[k]];
c2[k_]:= -kp[k]Log[g0[k]]/Power[g0[k],kp[k]];
pow1[k_]:= 1-k;
pow2[k_]:= -kp[k](1-k);
dt[k_,S0_][tau_] := tau-tau0[k,S0];
x1[k_,S0_][tau_] := Exp[pow1[k]dt[k,S0][tau]];
x2[k_,S0_][tau_] := Exp[pow2[k]dt[k,S0][tau]];
H2[k_,S0_][tau_] := HeavisideTheta[tau-tau0[k,S0]];
H1[k_,S0_][tau_] := 1-H2[k,S0][tau];
G[k_,S0_][tau_] := Gf[k]
 H1[k,S0][tau] b1[k] W[0,c1[k] x1[k, S0][tau]] +
 H2[k,S0][tau] (1-b2[k]W[0,c2[k]x2[k,S0][tau]]);

(* Analytical S,I,R,j,J as function of time t *)
(* parameters: k and S(t=0) *)
SIRS[k_,S0_][t_]:= Exp[-G[k,S0][tau[t]]];
SIRI[k_,S0_][t_]:= f[k][G[k,S0][tau[t]]];
SIRR[k_,S0_][t_]:= k G[k,S0][tau[t]];
SIRj[k_,S0_][t_]:= SIRS[k,S0][t]SIRI[k,S0][t];
SIRJ[k_,S0_][t_]:= 1 - SIRS[k,S0][t];

(* exact numerical result for comparison (via J) *)
exactSIRtauOfJ[k_,S0_][J_]:=
 NIntegrate[1/((1-y)(y+k Log[1-y])),{y,1-S0,J}];
exactSIRSofJ[k_,S0_][J_]:=1-J;
exactSIRIofJ[k_,S0_][J_]:=(k Log[1-J]+J);
exactSIRRofJ[k_,S0_][J_]:=-k Log[1-J];
exactSIRjofJ[k_,S0_][J_]:=(k Log[1-J]+J)(1-J);

(* example *)
(* j(t) for k=0.5 and S(t=0)=0.99 *)
Plot[SIRj[0.5,0.99][t],{t,-30,30}]

ParametricPlot[{exactSIRtauOfJ[0.5,0.99][J],
 exactSIRjofJ[0.5,0.99][J]},{J,0,Jf[0.5]}
```

1. L. Lixiang, Z. Yang, Z. Dang, C. Meng, J. Huang, H. Meng, D. Wang, G. Chen, J. Zhang, H. Peng, and Y. Shao. Propagation analysis and prediction of the covid-19. *Infect. Disease Model.*, 5:282–292, 2020.
2. I. Ciufolini and A. Paolozzi. Mathematical prediction of the time evolution of the covid-19 pandemic in italy by a gauss error function and monte carlo simulations. *Eur. Phys. J. Plus*, 135:355, 2020.
3. R. Schlickeiser and F. Schlickeiser. A gaussian model for the time development of the Sars-Cov-2 corona pandemic disease. predictions for Germany made on march 30. *Physics*, 2:164–170, 2020.
4. J. Schüttler, R. Schlickeiser, F. Schlickeiser, and M. Kröger. Covid-19 predictions using a gauss model, based on data from april 2. *Physics*, 2:197–202, 2020.
5. W. O. Kermack and A. G. McKendrick. A contribution to the mathematical theory of epidemics. *Proc. Royal Soc. A*, 115:700–721, 1927.
6. D. G. Kendall. Deterministic and stochastic epidemics in closed populations. In *Proc. Third Berkeley Symp. on Math. Statist. and Prob.*, volume 4, pages 149–165. Univ. of Calif. Press, Berkeley, United States, 1956.
7. H. W. Hethcode. The mathematics of infectious diseases. *SIAM Rev.*, 42:599–653, 2000.
8. S. M. O'Regan, T. C. Kelly, A. Korobeinikov, M. J. A. O'Callaghan, and A. V. Pokrovskii. Lyapunov functions for SIR and SIRS epidemic models. *Appl. Math. Lett.*, 23(4):446–448, 2010.
9. J. Satsuma, R. Willox, A. Ramani, B. Grammaticos, and A. S. Carstea. Extending the SIR epidemic model. *Physica A*, 336 (3-4):369–375, 2004.
10. M. Cadoni. How to reduce epidemic peaks keeping under control the time-span of the epidemic. *Chaos Soliton Fract.*, 138: 109940, 2020.
11. N. S. Barlow and S. J. Weinstein. Accurate closed-form solution of the sir epidemic model. *Physica D*, 408:132540, 2020.
12. N. S. Barlow, C. R. Stanton, N. Hill, S. J. Weinstein, and A. G. Cio. On the summation of divergent, truncated, and underspecified power series via asymptotic approximants. *Quart. J. Mech. Appl. Math.*, 70:21, 2017.
13. M. Cadoni and G. Gaeta. Size and timescale of epidemics in the sir framework. *Physica D*, 411:132626, 2020.
14. A. Chekroun and T. Kuniya. Global threshold dynamics of an infection age-structured sir epidemic model with diffusion under the dirichlet boundary condition. *J. Diff. Eq.*, 269(8):117–148, 2020.
15. C. Imron, Hariyanto, M. Yunus, S. D. Surjanto, N. A. C. Dewi, and Iop. *Stability and persistence analysis on the epidemic model multi-region multi-patches*, volume 1218 of *J. Phys. Conf. Ser.* 2019.
16. P. T. Karaji and N. Nyamoradi. Analysis of a fractional SIR model with general incidence function. *Appl. Math. Lett.*, 108: 106499, 2020.
17. Y. Mohamadou, A. Halidou, and P. T. Kapen. A review of mathematical modeling, artificial intelligence and datasets used in the study, prediction and management of Covid-19. *Appl. Intell.*, 2020. doi:10.1007/s10489-020-01770-9.
18. S. Samanta, B. Sahoo, and B. Das. Dynamics of an epidemic system with prey herd behavior and alternative resource to predator. *J. Physics A*, 52(42):425601, 2019.
19. N. Sene. SIR epidemic model with mittag-leffler fractional derivative. *Chaos Solit. Fract.*, 137:109833, 2020.
20. M. Simon. SIR epidemics with stochastic infectious periods. *Stoch. Proc. Appl.*, 130(7):4252–4274, 2020.
21. C. R. Tian, Q. Y. Zhang, and L. Zhang. Global stability in a networked SIR epidemic model. *Appl. Math. Lett.*, 107:106444, 2020.
22. G. D. Barmparis and G. P. Tsironis. Estimating the infection horizon of covid-19 in eight countries with a data-driven approach. *Chaos Solit. Fract.*, 135:109842, 2020.
23. U. Kolberg and R. Schlickeiser. Kinetic theory of small-amplitude fluctuations in astrophysical plasmas. *Phys. Rep.*, 783: 1–84, 2018.
24. T. Harko, F. S. N. Lobo, and M. K. Mak. Exact analytical solutions of the susceptible-infected-recovered (SIR) epidemic model and of the SIR model with equal death and birth rates. *Appl. Math. Comput.*, 236:184–194, 2014.
25. M. Kröger and R. Schlickeiser. Gaussian doubling times and reproduction factors of the Covid-19 pandemic disease. *Frontiers Phys.*, 8:276, 2020.
26. J. H. Lambert. Observations variae in mathesin puram, acta helvitica. *Physico-mathematico-anatomico-botanico-medica*, 3: 128–168, 1758.
27. R. M. Corless, G. H. Gonnet, D. E. G. Hare, D. J. Jeffrey, and D. E. Knuth. On the Lambert W function. *Adv. Computat. Math.*, 5(4):329–359, 1996.
28. D. A. Barry, J. Y. Parlange, L. Li, H. Prommer, C. J. Cunningham, and E. Stagnitti. Analytical approximations for real values of the Lambert W-function. *Math. Comp. Simul.*, 53(1-2):95–103, 2000.
29. F. Chapeau-Blondeau and A. Monir. Numerical evaluation of the Lambert W function and application to generation of generalized Gaussian noise with exponent 1/2. *IEEE Trans. Signal Proc.*, 50 (9):2160–2165, 2002.
30. A. Jain and A. Kapoor. Exact analytical solutions of the parameters of real solar cells using Lambert W-function. *Solar Energy Mater. Solar Cells*, 81(2):269–277, 2004.
31. S. R. Valluri, D. J. Jeffrey, and R. M. Corless. Some applications of the Lambert W function to physics. *Canad. J. Phys.*, 78(9): 823–831, 2000.
32. T. C. Scott, G. Fee, J. Grotendorst, and W. Z. Zhang. Numerics of the generalized Lambert W function. *SIGSAM*, 48:4256, 2014.
33. T. C. Scott, G. Fee, and J. Grotendorst. Asymptotic series of generalized Lambert W function. *SIGSAM*, 47:7583, 2013.